Tapping hydrogen fuel from the ocean : a review on photocatalytic, photoelectrochemical and electrolytic splitting of seawater

Tapping hydrogen fuel from the ocean:

a review on photocatalytic, photoelectrochemical and electrolytic splitting of seawater

Fons Dingenen,[a,b] Sammy W. Verbruggen[a,b,*]

[a] Sustainable Energy, Air & Water Technology (DuEL), University of Antwerp, Groenenborgerlaan 171, 2020 Antwerp, Belgium

[b] NANOlab Center of Excellence, University of Antwerp, Groenenborgerlaan 171, 2020 Antwerp, Belgium

* corresponding author details, Sammy.Verbruggen@uantwerpen.be, +323 265 32 60

Abstract

Direct splitting of earth-abundant seawater provides an eco-friendly route for the production of clean H_2, but is hampered by selectivity and stability issues. Direct seawater electrolysis is the most established technology, attaining high current densities in the order of 1-2 $A.cm^{-2}$. Alternatively, light-driven processes such as photocatalytic and photoelectrochemical seawater splitting are particularly promising as well, as they rely on renewable solar power. Solar-to-Hydrogen efficiencies have increased over the past decade from negligible values to about 2%. Especially the absence of large local pH changes (in the order of several tenths of a pH unit compared to up to 9 pH units for electrolysis) is a strong asset for pure photocatalysis. This may lead to less adverse side-reactions such as Cl_2 and ClO^- formation, (acid or base induced) corrosion and scaling. Besides, additional requirements for electrolytic cells, *e.g.* membranes and electricity input, are not needed in pure photocatalysis systems. In this review, the state-of-the-art technologies in light-driven seawater splitting are compared to electrochemical approaches with a focus on sustainability and stability. Promising advances are identified at the level of the catalyst as well as the process, and insight is provided in solutions crossing different fields.

Highlights

- Review on electrolytic, photocatalytic and photoelectrochemical seawater splitting
- Activity, selectivity, stability and sustainability of all technologies are compared
- Electrolysis is more mature, while photocatalysis may experience less side effects
- Promising solutions across fields are identified

Keywords

Seawater splitting; Hydrogen; Photocatalysis; Photoelectrochemical Cells, Electrolysis, Chloride

Word count: 10564

List of abbreviations

Abbreviations

AEC   Alkaline Electrolysis Cell

AEM   Anion Exchange Membrane

AQY   Apparent Quantum Yield

AM   Air Mass

BCC   Basic Cobalt Carbonate

BOP   Balance of Plant

CB   Conduction Band

CD   Carbon Dot

ClER Cl_2 Evolution Reaction

COF   Covalent organic framework

COP   Covalent organic polymers

CPS   Current Policies Scenario

DI   Deionized

EC   Electrolysis Cell

EDX   Energy Dispersive X-ray

FE   Faradaic efficiencies

GC   Gas Chromatography

HER   Hydrogen Evolution Reaction

IEA   International Energy Agency

LCOH   Levelized Cost of Hydrogen

LbL   Layer-by-Layer

LDH   Layered Double Hydroxide

(L)SPR   (Localized) Surface Plasmon Resonance

$LOCH_{PV}$ Photovoltaics derived Levelized Cost of Hydrogen

M   Metal

PEC   Photoelectrochemical

PEMEC Polymeric Electrolyte Membrane Electrolysis Cell

PGM   Platinum Group Metal

RH   Relative Humidity

1	RHE	Reversible Hydrogen Electrode
2	ROS	Reactive Oxygen Species
3	SC	Semiconductor
4	SEM	Scanning Electron Microscopy
5	SHE	Standard Hydrogen Electrode
6	SO	Solid Oxide
7	STH	Solar-to-Hydrogen
8	tj-a-Si	Triple junction amorphous Si
9	UV	Ultraviolet
10	VB	Valence Band
11	VIS	Visible light
12	VOC	Volatile Organic Compound

Nomenclature

14	ΔG	Gibbs free energy
15	ΔH	Enthalpy change
16	C	concentration
17	c	speed of light
18	E	Energy content
19	$E°$	Redox potential
20	E_g	Band gap energy
21	η	Overpotential
22	L	Length
23	N	Number
24	h	Planck's constant
25	h^+	Hole
26	j	Current density
27	λ	Incident light wavelength
28	v	Incident light frequency
29	P	Energy intensity
30	R	Reaction rate
31	S	Surface area

1	T	Temperature
2	t	Time
3	$t_{>90\%}$	Time before the initial activity drops 10%
4	θ	Angle
5	Units	
6	°C	Degrees Celsius
7	A	Ampere
8	atm	Standard atmosphere
9	$g_{(cat)}$	Gram (of catalyst)
10	h	Hour
11	J	Joule
12	m	Meter
13	M	Molar
14	mol	Mole
15	ppb	Parts per billion
16	ppm	Parts per million
17	sccm	Standard cubic centimeters per minute
18	t	Ton
19	V	Volt
20	W	Watt
21	wt%	Weight percentage
22		
23		
24		

Content

1. Introduction

Sufficient energy supply is one of the major issues in our growing modern society. In 2016, the world's energy consumption already amounted to 577.92 EJ. Of this value, 81% was delivered by non-sustainable fossil fuels, resulting in a global CO_2 emission of 32.1 Gt. The International Energy Agency (IEA) forecasted that the global energy demand will exceed 810 EJ following the current policies scenario (CPS) [1]. This will most probably give a strong driving force for global warming if no additional measures are taken. In order to meet the scenario in which the temperature rise stays below 2°C, renewable energy sources must play a more important role. The largest disadvantage of these resources is their variable nature over short periods of time, and the fact that the energy production and demand are not at all perfectly synchronized [2]. In that context the scientific community is showing ever-increasing interest in sustainable energy carriers such as H_2 to store and buffer the fluctuations in energy production and demand. This molecule is recognized worldwide as a promising energy vector. It benefits from a high energy conversion efficiency and ease of conversion in different forms of energy [3,4]. Besides, the required infrastructure, skills and regulations are already (partly) available. *E.g.* 40% of the European households already uses gas heating systems, that could allow H_2 usage as well. Hydrogen storage is often more cost efficient than battery storage and recharges 15 times faster, leading to smaller charging infrastructure [5]. The major downside is that nowadays, it is still produced for about 95% from fossil fuels since other production technologies are not yet fully mature [6]. Nonetheless, direct water splitting technologies are heavily studied to provide a short-to-medium term solution. In these technologies H_2 and O_2 are simultaneously evolved from water molecules (eq. 1), with basically no undesired side-reactions [4]. It is even stated by Hydrogen Europe that without water-derived H_2, deep decarbonization (>80%) will be impossible [5].

$$2\ H_2O\ (l) \rightarrow 2H_2\ (g) + O_2\ (g)\ (\Delta H= 286\ kJ.mol^{-1}) \tag{1}$$

With ΔH the change in enthalpy.

Electrochemical methods are considered as one of the most efficient ways to provide the required energy for this endothermal reaction. In addition, since solar power is the most abundant renewable energy source (every second about 1.2×10^{14} kJ reaches the Earth's surface [7]) photoelectrochemical (PEC) and direct photocatalytic water splitting are studied extensively as well [8]. It is even called one of the 'Holy Grails' of chemistry [9]. Next to energy, the other crucial resource is water. Unfortunately, considering the population growth, the availability of fresh water as a feedstock becomes problematic. Hence, it would be better to use abundant seawater, that accounts for *ca*. 97% of the water on Earth [10]. Another advantage is the fact that (sea)water is quite evenly distributed throughout the globe, allowing to decrease the dependence on fossil fuel producing countries [10]. On the other hand, the use of seawater imposes important technological challenges due to the abundant presence of various ions (Table 1), averaging 3.5 wt% in total [10].

1   Table 1: Ion concentrations (*C*) in standard seawater. Based on values from Ref. [10].

Solute (ion)	C (g.kg^{-1} seawater)
Cl$^-$	20.058
Na$^+$	11.177
SO$_4^{2-}$	2.812
Mg^{2+}	1.331
Ca^{2+}	0.427
K$^+$	0.414
HCO$_3^-$	0.112
Br$^-$	0.070
B(OH)$_3$	0.020
CO$_3^{2-}$	0.016
Sr^{2+}	0.008
B(OH)$_4^-$	0.008
F$^-$	0.001

2

3   Both photocatalytic as well as (photo)electrochemical seawater splitting research has been evolving
4   rapidly over the last years. While a very limited number of overview articles is available on one given
5   technology in particular [11–13], to the best of our knowledge a concise, comparative overview of
6   the current state of the art in these different fields is lacking. In this review these technologies will be
7   compared, starting from their basic fundamental principles, followed by a comparison between their
8   overall efficiencies and resulting costs for H$_2$ production. In subsequent sections, the seawater
9   selectivity, stability and other influencing factors will be discussed in more detail. A particular focus
10   lies on recent technological developments for dealing with saline media in view of their application in
11   seawater. Note that in this review only direct seawater utilization is considered, *i.e.* without prior
12   desalination of the water. Certainly in applications with space constraints (*e.g.* ships), a prior
13   desalination step would be inadvisable [10]. Besides, more specific (bio-based) niche-technologies
14   such as microbial processes with cyanobacteria [14], phototrophic [15] and dark-acidogenic bacteria
15   [16], the decomposition of H$_2$S from the Black Sea [17] and the hydrolysis of Mg species in seawater
16   [18] are not considered in this overview. The interested reader is kindly referred to the
17   corresponding references, as well as an excellent review article by Fukuzumi *et al.* (2017) [19].

18   ## 2. Basic principles
19   The following section briefly discusses the fundamentals behind electrolytic, photocatalytic and
20   photoelectrochemical water splitting. Readers already familiar with the basic principles of each
21   technology are welcome to directly proceed to the next section.

22   ### 2.1 Electrolytic water splitting
23   Volta was probably one of the first to open up the electrolysis research domain with the discovery of
24   his voltaic pile in 1799. A few months later, Carlisle and Nicholson applied this setup for the first time
25   as a water splitting electrolysis cell (EC) [20]. The pile consisted of a series of copper and zinc plates
26   (the electrodes) separated by cardboard layers soaked in salt water (the electrolyte) [21,22]. In a

1 standard EC, an external voltage is applied to the electrodes to drive the different redox half
2 reactions. These electrodes are connected by an electronic circuit to enable the flow of electrons.
3 The ionic conductivity is further guaranteed by the electrolyte [23]. Nowadays, different types of ECs
4 exist with low temperature acidic polymeric electrolyte membrane ECs (PEMECs, Fig. 1a) and liquid
5 electrolyte alkaline ECs (AECs) as the most established ones [10]. Other types of ECs such as anion
6 exchange membrane (AEM) and high temperature solid oxide (SO) ECs will not be discussed here in
7 detail for the sake of brevity. The reader is kindly referred to the reviews of Vincent *et al.* (2017) [24]
8 and Laguna-Bercero (2012) [25] for more information on those particular topics. The extreme pH
9 conditions in simple PEMECs and AECs result from the addition of strong electrolytes like H_2SO_4 or
10 NaOH and KOH [26]. Note that their addition is not strictly required in seawater due to the natural
11 occurrence of ions. Nonetheless, it is still often done to increase the ionic conductivity [27–29]. At
12 the anode in a PEMEC, water is oxidized to oxygen (Oxygen Evolution Reaction, OER, eq. 2). The
13 released electrons and protons are then transferred to the cathode via the electronic circuit and the
14 polymeric membrane, respectively. Here, they combine to form H_2 (Hydrogen Evolution Reaction,
15 HER, eq. 3). In AECs on the other hand, hydroxide anions are oxidized to oxygen gas at the anode (eq.
16 4) and water is reduced at the cathode (eq. 5) [7].

17 Acidic OER: $2\ H_2O\ (l) \rightarrow O_2\ (g) + 4\ e^- + 4\ H^+$ (2)
18 Acidic HER: $4\ e^- + 4\ H^+ \rightarrow 2\ H_2\ (g)$ (3)
19 Basic OER: $4\ OH^- \rightarrow O_2\ (g) + 2\ H_2O\ (l) + 4\ e^-$ (4)
20 Basic HER: $4\ H_2O\ (l) + 4\ e^- \rightarrow 2\ H_2\ (g) + 4\ OH^-$ (5)

21 The absolute minimum theoretical voltage is 1.23 V *vs.* SHE (Standard Hydrogen Electrode) for water
22 splitting at room temperature. This corresponds to the difference between the redox potentials of
23 the respective half reactions at a given pH. However, a larger potential is applied to ensure a
24 sufficient reaction rate, denoted as the 'overpotential' (η). Obviously, the goal is to minimize this
25 excess energy, which is the role of the electrocatalyst [7]. For PEMECs, the best performing
26 electrocatalysts are Platinum Group Metals (PGMs) (Pd > Pt ≈ Rh > Ir > Re > Os > Ru > Ni) at the
27 cathode and IrO_2 or RuO_2 at the anode [30]. In AECs, mostly first row transition metals (*e.g.* Ni, Mn,
28 Fe, Co *etc.*) or their alloys are used as electrocatalysts for the HER [7], while oxides or
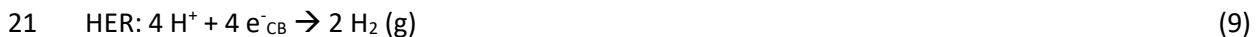29 (oxy)hydroxides are found at the anode [31].
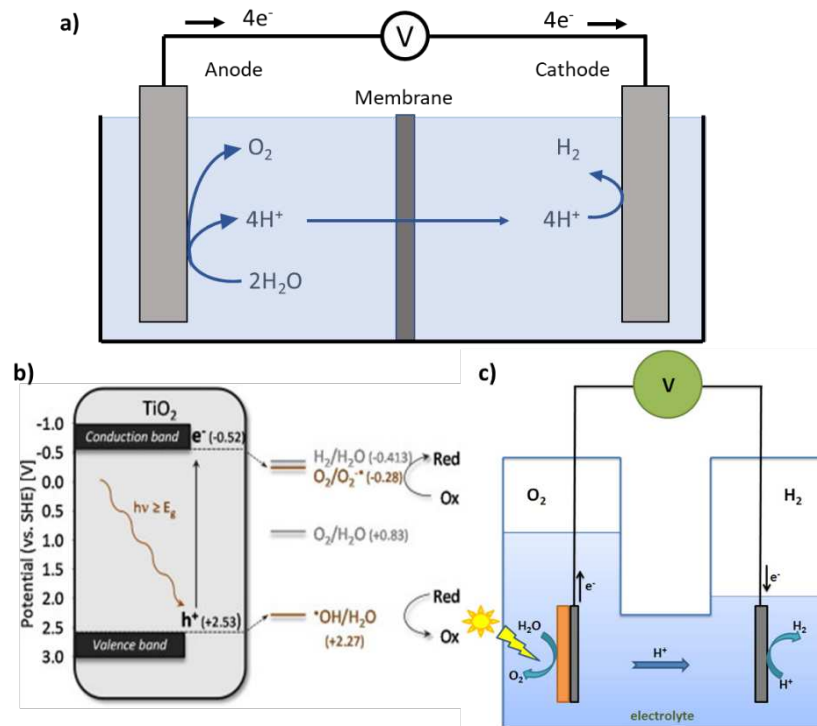
2.2 Photocatalytic water splitting

Photocatalysis research started nearly two centuries after the discovery of electrolysis. In 1972, Fujishima and Honda observed for the first time the water splitting capacity of TiO$_2$ under ultraviolet (UV) irradiation [34]. In this domain, semiconductors (SC) catalyze redox reactions such as the HER and OER simultaneously under illumination. This ability originates from their specific electronic band structure, that consists of a filled valence band (VB) and an empty conduction band (CB) with a small bang gap (E_g) in-between. When the semiconductor is illuminated by light of sufficient energy to overcome the band gap, an electron of the VB is excited to the CB (e^-_{CB}), leaving behind a positively charged hole in the VB (h^+_{VB}) (eq. 6) [35]. The required wavelength for this excitation is determined by the Einstein-Planck relation (eq. 7) [32]. After migrating to the catalyst surface, the holes can initiate water oxidation (eq. 8), while the conduction band electrons initiate the reduction of protons (eq. 9) [32].

SC + $h.v$ → h^+_{VB} + e^-_{CB}	(6)
$E = h.v = h.c/\lambda$ > E_g	(7)
OER: 2 H$_2$O (l) + 4 h^+_{VB} → O$_2$ (g) + 4 H$^+$	(8)
HER: 4 H$^+$ + 4 e^-_{CB} → 2 H$_2$ (g)	(9)

With h Planck's constant (6.63×10^{-34} J.s), v the incident light frequency, E the energy content, c the speed of light (300×10^6 m.s^{-1}), λ the incident light wavelength and E_g the band gap.

Whether a SC is suitable for un-biased photocatalytic water splitting is largely determined by the respective positions of the VB and CB edges. The redox potentials of the photogenerated h^+_{VB} and e^-_{CB} need to be more positive and more negative than those of the water oxidation and reduction half reactions, respectively. These correspond resp. to +0.83 V vs. SHE and -0.41 V vs. SHE at neutral pH [32]. Band gaps should evidently always be greater than 1.23 eV. The optimal value is determined by

the availability of sunlight. It is therefore beneficial to have a band gap in the order of 2.53 eV which matches the wavelength range of maximum solar intensity at the Earth's surface (around 490 nm) [36].

The most common SC is the relatively cheap, chemically stable TiO_2 ($E_g \approx$ 3.0-3.2 eV, Fig. 1b). This photocatalyst guarantees water splitting due to its sufficiently strong oxidant h^+_{VB} (2.53 V > 0.83 V vs. SHE) and reductant e^-_{CB} (-0.52 V < -0.41 V vs. SHE) [32]. One of the first main drawbacks of TiO_2 is its fairly large band gap, that requires excitation by UV light. Other suitable SCs include several oxides, (oxy)sulfides and (oxy)nitrides with d^{10} cations (*e.g.* Ga^{3+}, Ge^{4+}, In^{3+}, Sb^{5+}, Sn^{4+}) or d^0 transition metal cations (*e.g.* Mo^{6+}, Nb^{5+}, Ta^{5+}, Ti^{4+}, W^{6+}, Zr^{4+}) [37]. Also Metal Organic Frameworks (MOFs) are studied for their photocatalytic activity. Note that other factors such as diffusion lengths and efficient separation of the charge carriers are important as well. The more efficient, the less recombination of the photogenerated charge carriers occurs (eq. 10). Recombination processes result in a dramatic decrease in efficiency [32].

$h^+_{VB} + e^-_{CB} \rightarrow$ energy   (10)

2.3 PEC water splitting
PEC water splitting is situated at the intersection of ECs and photocatalysis. A basic PEC cell configuration (Fig. 1c) consists of a cathode and an anode submerged in an aqueous electrolyte solution [26]. Alike ECs, both electrodes are connected by an external electronic circuit. The difference with ECs lies in the fact that one or two electrodes are photoactive [26]. Important materials for photoanodes and -cathodes are n-type (*e.g.* TiO_2 [38]) and p-type semiconductors (*e.g.* Cu_2O [39]), respectively. Depending on these photocatalysts, a suitable electrolyte is chosen. For example, alkaline electrolytes are the most optimal for TiO_2 anodes [26]. If non-photoactive counter electrodes are used, they often consist of Pt [26].

When wide band gap SCs such as TiO_2 are utilized, an additional voltage or bias is often applied. This is done when the band edges are not suitable for water splitting (*e.g.* in the case of WO_3) [40]. In that case, the photoelectrodes also contain an electrocatalyst to minimize the overpotential [41]. The need for additional energy and other issues will be thoroughly discussed in the following section. A comparison between the different technologies will be made with special attention to the technical issues arising when using seawater.

3. Comparison
Firstly, the efficiencies that can be attained to date are presented for both technologies. Hereafter, a closer look is taken at the different factors that may influence the efficiency, going from selectivity over stability-related problems, to additional operational requirements. Recent interesting improvements on the level of the catalyst or the reactor will be discussed when relevant.

3.1 H_2 evolution efficiencies and costs
3.1.1 Electrolysis
Water electrolyzers already perform quite efficiently. The efficiency of mature pure water AECs with a capacity up to 150 MW reaches 82%, while the early market PEMECs (< 1 MW) have a 65-78% efficiency [42]. Direct seawater electrolysis on the other hand, attains voltage efficiencies based on the H_2 higher heating value (141.5 MJ.kg^{-1}) up to 79% [29]. This is yet similar to the 70-85% range of the industrial large scale steam methane reformers (SMR) (150-300 MW) [42]. Although the efficiencies are similar, the costs differ significantly. SMR-derived H_2 costs about US$ 1.25 kg^{-1} for a natural gas price of US$ 3.50 GJ^{-1}. Nowadays, large scale electrolysis plants operate solely on pure water, yielding H_2 at a cost of *ca.* US$ 4.09 kg^{-1} (coal-powered) [43]. This is slightly above the US

1 Department of Energy (DOE) goal of US\$ 2.00-4.00 kg^{-1}. The H$_2$ cost consists of the complete power-
2 to-gas installation investment costs (US\$ 2009 kW^{-1} on average), operational costs (US\$ 39.5 kW^{-1}),
3 energy costs and water costs (*ca.* US\$ 0.08 kg^{-1}) [44,45]. In contrast to PV-derived H$_2$ (> US\$ 5 kg^{-1}
4 [43]), small-scale wind energy powered H$_2$ production may already hit this target in specific cases
5 (US\$ 3.53 .kg^{-1} in Texas) [44]. However, as mentioned earlier, this is only valid when working with
6 pure water. Accurate techno-economic assessments for direct seawater electrolysis are still non-
7 existent and strongly requested. The use of seawater may drastically decrease the cost of water, but
8 increase the electrolyzer costs (*e.g.* operational EC cost is estimated to increase ≥6-fold without
9 proper stabilization) [13]. d'Amore-Domenech *et al.* (2020) recently estimated that the lifetime of
10 conventional PGM electrodes would decrease by at least an order of magnitude [13]. Seawater
11 causes several detrimental effects such as Cl$_2$ evolution [46], scaling [47], fouling of membranes [48],
12 corrosion [46] *etc.* which is especially true for PEMECs that require very pure water [7]. Ren's group
13 recently attained very promising results for alkaline seawater splitting, similar to pure water splitting.
14 Their 3-dimensional core shell metal nitride electrocatalyst achieved industrially required current
15 densities of 500 and 1000 mA.cm^{-2} at record low voltages of 1.608 V and 1.709 V, respectively (Fig.
16 2a). These results emphasize the potential this research domain has to offer [27]. To complete the
17 overview, a selection of recently developed HER and OER electrocatalysts is presented in Table 2 with
18 parameters quantifying their activity, selectivity and stability in seawater. From this table, it is clear
19 that nowadays already low overpotentials (70-480 mV) allow to operate the HER at useful current
20 densities of about 10 mA.cm^{-2}. The OER generally requires higher overpotentials. Finally, it is
21 important to notice that both half reactions can be performed using sustainable PGM-free catalysts,
22 like Ni. The selectivity and stability will be discussed further in the following paragraphs.

23
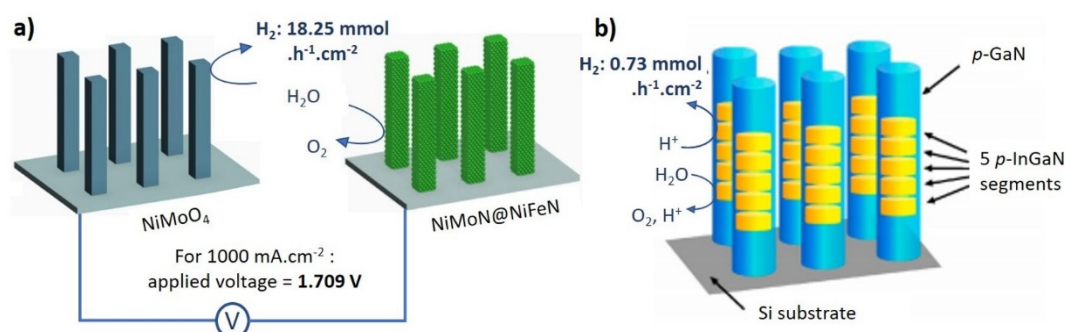
24
25 Figure 2: Configuration and H$_2$ yield for a) Ren's electrocatalysts and b) Guan's photocatalyst (at 27 sun) in seawater. The H$_2$
26 yields are normalized for the substrate surface area. Adapted with permission from resp. Ref.[27], Copyright (2019) CC BY
27 4.0 and Ref. [49] Copyright (2018) American Chemical Society.

28 Table 2: Overpotentials (η) with their current densities (*j*), reaction media, Faradaic efficiencies (FE) and the time before
29 the initial activity drops 10% (t$_{>90\%}$) for recently studied HER and OER electrocatalysts

Electrocatalyst Working electrode	Counter electrode	Reaction medium (pH[a])	η (mV) (for *j*[b])	FE[c]	t$_{>90\%}$ (h)	Ref.
			HER			
Ti/NiPt	Pt foil	Natural seawater	~342 (10 mA.cm^{-2})	NA	~10	[50]
PtMo$_{0,1}$ on Ti mesh	Pt foil	Natural seawater	255 (10 mA.cm^{-2})	NA	172	[51]
Mn doped NiO/Ni	graphite rod	Natural seawater (pH 8.20)	170 (10 mA.cm^{-2})	~100% (1h) ~70% (7h)[d1]	<2	[52]
NiMoN	NiMoN@	Natural seawater +	82 (100 mA.cm^{-2})	97.8%[d1]	48	[27]

	NiFeN	1 M KOH (pH 14)				
NiMoS on C fiber cloth	graphite foil	Natural seawater (pH 7)	200 (10 mA.cm^{-2})	98.2%[d1]	NA	[53]
NiFeC on Co foil	Pt sheet	Artificial seawater at 90°C (pH 12.00)	70 (12 mA.cm^{-2})	NA	NA	[54]
Co$_3$Mo$_3$C/CNT/Ni foam	Pt sheet	Natural seawater (pH 6.44)	124 (10 mA.cm^{-2})	NA	26	[55]
CoSe$_4$ on Co foil	C	Natural seawater (pH 7.4)	268 (100 mA.cm^{-2})	NA	<1	[56]
CoMoP@C core-shell	graphite rod	Natural seawater (pH 8.35)	~479 (10 mA.cm^{-2})	92.5%[d1]	10[e]	[57]
Urea derived CNTs	C rod	Natural seawater (pH 7.00)	250 (10 mA.cm^{-2})	~100%[d1]	7	[58]
Mo$_5$N$_6$ nanosheets on glassy carbon	graphite counter rod	Natural seawater (pH 8.40)	257 (10 mA.cm^{-2})	NA	>40[f]	[59]
FeO$_x$	FeO$_x$	Artificial seawater + 0.1 M KOH (pH 13)	400 (10 mA.cm^{-2})	~100%[d1]	72	[60]

OER						
NiMoN@NiFeN	NiMoN	Natural seawater + 1 M KOH (pH 14)	369 (500 mA.cm^{-2})	97.8%[d1]	48	[27]
NiFe/NiS$_x$/Ni foam	Ni/NiO/ Cr$_2$O$_3$	Artificial seawater + 1 M KOH (pH 14)	300 (400 mAcm^{-2})	~100%[d1]	1000	[46]
NiFe layered double hydroxide	Pt mesh	Artificial seawater + 0.1 M KOH (pH 13)	359 (10 mA.cm^{-2})	~100%[d2]	~2	[47]
NiFe layered double hydroxide	Pt mesh	Artificial seawater + 0.3 M borate buffer (pH 9.2)	490 (10 mA.cm^{-2})	~100%[d2]	~0,75	[47]
Basic Co carbonate @Co$_2$[Fe(CN)$_6$] core-shell	NiMoS	Natural seawater (pH 7)	350 (10 mA.cm^{-2})	100%[d3]	100	[61]
MnO$_x$/IrO$_x$/glassy C	Pt ring	Artificial seawater (pH 0.88)	300 (5 mA.cm^{-2})	93%[d4]	~0.03	[62]

[a] if known

[b] Note that 10 mA.cm^{-2} corresponds to a H$_2$ of 1.86 µmol.h^{-1}.cm^{-2} if a FE of 100% is assumed. FE refers to the fraction of generated electrons effectively used for H$_2$ evolution during HER.

[c] FE referring to resp. H$_2$ and O$_2$ generation for HER and OER electrocatalysts.

[d1] determined using gas chromatography (GC); [d2] determined using electrochemical online mass spectrometry; [d3] determined using a volumetric method; [d4] determined using rotating ring-disk electrode for quantitative measurement of Cl$_2$ (complementary to O$_2$ evolution)

[e] disregarding initial overshoots

[f] for η is 300 mV

3.1.2   Photocatalytic and PEC seawater splitting

The H$_2$ yields obtained through electrolytic water splitting are not yet achieved by direct photocatalytic processes. The major reason being the limited available natural solar power, in the order of 100 mW.cm^{-2}, commonly denoted as an irradiation intensity of '1 sun'. The DOE targeted a Solar-to-Hydrogen (STH) efficiency of 10% as the benchmark for commercialization [40]. This STH can be described according to eq. 11 [63]:

$$STH\ (\%) = \frac{output\ energy\ in\ H_2}{input\ solar\ energy} = \frac{R_{H_2}.\Delta G}{P.S}.100\%$$

(11)

With R_{H2} the H$_2$ evolution rate, ΔG the Gibbs free energy for the water splitting reaction, P the energy intensity of the used illumination and S the illuminated surface area.

For 1 sun illumination and based on the Gibbs free energy (237.13 MJ.kg^{-1} at 25°C and 1 atm) this corresponds to a H$_2$ production rate of ~150 μmol.h^{-1}.cm^{-2} or a photocurrent density of ~8 mA.cm^{-2} for PEC cells with a theoretical maximal Faradaic efficiency of 100% [64]. To achieve such high efficiency, photocatalysts should be developed with an absorption edge higher than 600 nm and an apparent quantum yield (AQY) of 60% [65] which is calculated as in eq. 12:

AQY = (number of used electrons for H$_2$)/(number of incident photons) = (2.N$_{H2}$)/N$_{photons}$ (12)

With N_{H2} and $N_{photons}$ the number of generated H$_2$ molecules and incident photons, respectively.

These targets have not yet been attained in this young research field. In general, STH efficiencies of direct photocatalysis often stay one order of magnitude lower, around 1% [63]. This is mostly due to the use of large band gap SCs, recombination, back reactions and poisoning with peroxo-compounds [66]. Yet, promising results have recently been reported using both pure water and seawater. Liao *et al.* (2013) obtained STH efficiencies in the order of 5% in pure water with earth abundant CoO photocatalysts [67], while Guan *et al.* (2018) achieved a stable 1.9% efficiency in seawater using p-GaN-based nanowire arrays under concentrated sunlight (Fig. 2b) [49]. Besides, several recent studies with less intense light sources yielded STH efficiencies of ~2% [68,69]. Moreover, Jaramillo and co-workers estimated that the cost of H$_2$ could even drop to US$ 1.6-3.8 kg^{-1} [43]. This is well below the DOE target. Pure photocatalysis would thus outperform current PEC water splitting (US$ 4.2-10.4 .kg^{-1} H$_2$) due to its simpler design [43], despite the difficulties concerning catalyst immobilization and recovery [70]. Note that over 80% of this maximal cost for PEC water splitting comes from the materials, construction and installation of the PEC cells [43]. Regardless of the higher cost, PEC cells are still promising because of their ability to reach high STH efficiencies. The theoretical maximum for a single cell lies at 16.8% given minimal ohmic and kinetic losses [71]. Even higher efficiencies are theoretically possible by using tandem cells [40]. Interesting results in that context were obtained at Rutgers in 2018. A STH efficiency of 11.5% could be reached using a Ni$_5$P$_4$ HER catalyst attached to a high performing p-GaInP$_2$/GaAs photoabsorber in pure water. The system was covered with a TiN protection layer possibly allowing the use in more harsh environments [72]. If the STH efficiency of a tandem cell would reach 25%, the levelized cost of hydrogen (LCOH) could even decrease to US$ 2.90 kg^{-1}. This should be possible in theory using appropriate triple junction cells [43].

A wide selection of photocatalytic and PEC seawater splitting studies are provided in Table 3 and Table 4, respectively. A very important critical note has to made here, stating that comparisons between different studies are often strongly hampered by the use of different light sources and intensities, especially in pure photocatalysis research. Therefore, it would be very useful if standard testing protocols became more established. A good first measure would be to use 100 mW.cm^{-2} (1

sun) Air Mass (AM) 1.5G simulated solar light in all setups. From the studies using *ca.* 1 sun illumination, it is clear that H_2 yields range from 0.8 to 5 mmol.h^{-1}.g_{cat}^{-1}. Besides, it seems that the yields for oxides and nitrides are lower than those for sulfide-modified photocatalysts which is in accordance with the size of the band gaps. In contrast to pure photocatalysis, PEC cells are easily compared to ECs due to the similar setup. It is clear that the PEC photocurrent densities are limited to an order of magnitude of 10 mA.cm^{-2}. This is still 50-200 times smaller than for the most advanced ECs. Consequently, larger surface areas will be required for industrial operation, while several other parameters such as seawater selectivity and stability should also be considered. These will be dealt with in the following paragraphs.

Table 3: Summary of several photocatalyst studies in seawater, presented with the used light, reaction medium, H_2 yield (in mmol H_2 per gram catalyst per hour) and the time before activity drops max. 10% ($t_{>90\%}$)

Photocatalyst	Light (intensity[a])	Reaction medium (pH[a])	H_2 yield (mmol. g_{cat}^{-1}.h^{-1})	$t_{>90\%}$ (h)	Ref.
MoS$_2$/TiO$_2$	Solar (AM1.5G, 100 mW.cm^{-2})	Natural seawater + methanol (8:2 v:v) (pH 8.4)	3.43	21	[73]
2.5% CuO/nano TiO$_2$	UV-VIS	Artificial seawater	3.1 x10^{-3}	5	[74]
NiO/Ni/La$_2$Ti$_2$O$_7$	UV	Natural seawater (pH 8.5)	0.696	3	[75]
Pt/CdS/TiO$_2$	VIS (>420 nm)	Natural seawater + 10 mM Na$_2$S + 2 mM Na$_2$SO$_3$	1.86	3	[75]
Pt/TiO$_2$	UV-VIS (>320 nm, 558 mW.cm^{-2})	Natural seawater + 1.09 M glycerol (pH 7.7)	1.57	1	[76]
0.5 wt% Pt/TiO$_2$	UV-VIS (>320 nm, with UV: 2.52 mW.cm^{-2})	Artificial seawater + 10 mmol oxalic acid (natural pH)	2.66	<3	[77]
0.5 wt% Pt/TiO$_2$	UV-VIS (>320 nm, with UV: 2.52 mW.cm^{-2})	Artificial seawater + 17 mmol ethanol (pH 9.58)	3.60	<3	[77]
Ti^{3+} self-doped Ti-O-Si	VIS (>420 nm)	Artificial seawater + 10 vol% triethanolamine (pH 8.2)	1.93	28	[78]
Ti^{3+} self-doped Ti-O-Si	420 nm (3.15 mW.cm^{-2})	Artificial seawater + 10 vol% triethanolamine (pH 8.2)	0.236	10	[78]
Rutile TiO$_2$	UV-VIS	Artificial seawater + 200 kHz 200 W ultrasound	~0.184	3	[79]
(WS$_2$)$_{0,7}$/(C-TiO$_2$)$_5$/g-C$_3$N$_4$	Solar (AM1.5G, 117 mW.cm^{-2})	Natural seawater	4.56	5	[68]
(WS$_2$)$_{0,7}$/(C-TiO$_2$)$_5$/g-C$_3$N$_4$	420 nm (9.584 mW.cm^{-2})	Natural seawater	0.249	5	[68]
SiO$_2$/Ag@TiO$_2$ core shell	Solar (AM1.5G, 100 mW.cm^{-2})	Artificial seawater + 20% v/v glycerol (pH 7.99)	0.857	2	[80]
0.3 wt% Ni/NaTaO$_3$	UV-VIS	0.5 M NaCl + 0.1 M glucose	~23.4	NA	[81]
NiS/ZnS$_{1-x-0.5y}$O$_x$(OH)$_y$/ZnO	VIS (>420 nm)	Natural seawater + 24 g.L^{-1} Na$_2$S.9H$_2$O + 5 g.L^{-1} Na$_2$SO$_3$	0.333	12	[82]
(Ni–ZnO)@C nanoreactors	UV-VIS	Artificial seawater + 2% methanol	5.1 x10^{-3}	5	[83]

Catalyst	Light	Reaction medium (pH)	j	t	Ref.
Pt/Cd$_{0.5}$Zn$_{0.5}$S	VIS (>420 nm)	0.5 M NaCl + 0.05 M glucose (pH 12)	~0.183	20	[84]
Nanotube TiO$_2$/Pt/ Cd$_{0.8}$Zn$_{0.2}$S	UV-VIS (>395 nm)	Natural seawater+ Na$_2$S/Na$_2$SO$_3$ (pH 6.8)	5.1	6	[85]
Nanotube TiO$_2$/Pt/ Cd$_{0.8}$Zn$_{0.2}$S	UV-VIS (>395 nm)	Seawater + benzyl alcohol/acetic acid	21.7	6	[85]
ZnO/Pt/ Cd$_{0.8}$Zn$_{0.2}$S	UV-VIS (>395 nm)	Natural seawater+ Na$_2$S/Na$_2$SO$_3$ (pH 6.8)	16	6	[85]
ZnO/Pt/ Cd$_{0.8}$Zn$_{0.2}$S	UV-VIS (>395 nm)	Seawater + benzyl alcohol/acetic acid	21.7	6	[85]
Nanorod ZnO/Pt/ Cd$_{0.8}$Zn$_{0.2}$S	UV-VIS (>395 nm)	Seawater+ Na$_2$S/Na$_2$SO$_3$	11.8	6	[85]
Nanorod ZnO/Pt/ Cd$_{0.8}$Zn$_{0.2}$S	UV-VIS (>395 nm)	Seawater + benzyl alcohol/acetic acid	23.7	6	[85]
Eosin Y modified MoS$_2$	UV-VIS (>395 nm)	Seawater + triethanolamine	14.5	6	[85]
CdS	UV-VIS (>395 nm)	Natural seawater	0.207	6	[85]
Cd$_4$P$_2$Br$_3$	UV-VIS (>395 nm)	Natural seawater	0.010	6	[85]
C dots/CdS	Solar (AM1.5G, >420 nm)	Natural seawater + 10% lactic acid	4.64	12	[86]
Cd$_{0.25}$Zn$_{0.75}$Se/CoP	Solar (AM1.5G)	Artificial seawater	36.6	7.5	[87]
C dots/g-C$_3$N$_4$	Solar (AM1.5G, >420 nm, 70 mW.cm^{-2})	Seawater	~0.539	24	[66]
p-GaN/InGaN nanowire arrays	Solar (AM1.5G, 27 sun)	Artificial seawater (pH 7)	5.10 x10^3	3	[49]

1 ^{a} if known

2 Table 4: Summary of several PEC studies in seawater, presented with the used light, reaction medium, obtained current
3 densities (*j*) with the applied bias, Faradaic efficiencies (FE) and the time before activity drops max. 10% (t$_{>90\%}$).

Catalyst working electrode	Counter electrode	Light (intensity)	Reaction medium (pH^a)	*j* (mA.cm^{-2}) (bias)	FE^b	t$_{>90\%}$ (h)	Ref.
			HER				
Co$_3$O$_4$	Pt gauze	Solar (AM1.5G, 100 mW.cm^{-2})	Natural seawater (pH 7.69)	25 (0.830 V$_{RHE}$)	NA	0.5	[88]
p-Si/TiO$_2$/NiO$_x$	Pt	Solar (AM1.5G, 100 mW.cm^{-2})	Artificial seawater (pH 8.4)	10 (0.7 V$_{RHE}$); 20 (0.9 V$_{RHE}$)	91%^{c}	~5	[89]
			OER				
TiO$_2$	Pt	Solar (outdoor, 36.2 mW.cm^{-2})	Natural seawater	0.0947 (0 V$_{RHE}$)	NA	NA	[90]

CdS/TiO$_2$	Pt sheet	VIS (>400 nm, 100 mW.cm^{-2})	Artificial seawater	0.494 (NA)	NA	0.083^s	[91]
BiOI@Bi core-shell microspheres/ TiO$_2$ nanotube arrays	Pt sheet	Solar (AM1.5G, 100 mW.cm^{-2})	Artificial seawater (pH 7)	1.42 (1.23 V$_{RHE}$)	85.7%^{c}	4	[69]
Polyaniline-graphene oxide-TiO$_2$	Pt wire	UV-VIS (300 W Xe with VISREF filter, 320-780 nm, 503.2 mW.cm^{-2})	Artificial seawater	3.93 (0.6 V$_{Ag|AgCl}$)	NA	5	[92]
Co-Pi decorated TiO$_2$@g-C$_3$N$_4$ nanoarrays	Pt wire	Solar (AM1.5G, 100 mW.cm^{-2})	Natural seawater (pH 6.4)	1.6 (1.23 V$_{RHE}$)	NA	10	[93]
porous WO$_3$ films	Pt wire	Solar (AM1.5G, 100 mW.cm^{-2})	Natural seawater (pH 6.4)	1.95 (1.23 V$_{RHE}$)	NA	3	[94]
Nanostructured WO$_3$ films	Pt wire	Solar (AM1.5G, 100 mW.cm^{-2})	Artificial seawater (pH 2)	4.78 (0.95 V$_{RHE}$)	NA	<20	[95]
α-Fe$_2$O$_3$/WO$_3$ nanorod arrays	Pt foil	Solar (AM1.5G, 100 mW.cm^{-2})	Natural seawater (pH 6.8)	1.02 (1.23 V$_{RHE}$)	NA	~1	[96]
Ag/WO$_3$/ZnFe-LDH	Pt	Solar (AM1.5G, 100 mW.cm^{-2})	Natural seawater (pH 8.08)	1.18 (1.23 V$_{RHE}$)	~100%^{c}	~6.67^d	[97]
2D/2D WO$_3$/g-C$_3$N$_4$ nanosheet arrays	Pt wire	Solar (AM1.5G, 100 mW.cm^{-2})	Natural seawater (pH 6.4)	0.73 (1.23 V$_{RHE}$)	NA	1	[98]
RhO$_2$ loaded Mo-doped BiVO$_4$	Pt wire	Solar (AM1.5G, 100 mW.cm^{-2})	Natural seawater (pH 6)	2.16 (1.0 V$_{RHE}$)	20%^{c}	~3^d	[99]
Ag$_8$SnS$_6$	Pt sheet	Solar (AM1.5G, 100 mW.cm^{-2})	Artificial seawater (pH 7)	2.09 (0.9 V$_{RHE}$) 2.5 (1.23 V$_{RHE}$)	NA	<0.03	[100]

1 ^{a} if known
2 ^{b} FE referring to resp. H$_2$ and O$_2$ generation for HER and OER electrocatalysts.
3 ^{c} determined using GC
4 ^{d} disregarding initial overshoots

5 ### 3.2 Cl$_2$ and ClO$^-$ evolution

6 In the following section a closer look is taken at the selectivity of seawater splitting. Next to the OER,
7 detrimental competing oxidation reaction can occur. Especially Cl$^-$ chemistry plays a major role in
8 these systems. The selectivity for the OER is therefore far more challenging than for the HER. This
9 HER selectivity originates from its more optimal reduction potential compared to those of the main
10 seawater components [10]. Still, some anions such as NO$_3^-$ and IO$_3^-$ can reduce [101], but their
11 concentrations are negligible in seawater (below ppb [102] and ppm level [103], respectively). For
12 these reasons, the main focus lies on Cl$_2$ and ClO$^-$ evolution.

2   Competing reactions with Cl^- species are probably the most important complication for seawater
3   electrochemistry [47]. Based on the Pourbaix diagram (Fig. 3), one could state that at low pH values
4   the Cl_2 evolution reaction (ClER, eq. 13) is the main competing reaction, while at high pH values the
5   formation of the hypochlorite anion (eq. 14) prevails [47]. Next to being toxic and highly
6   environmentally unfriendly [104], these species are also disadvantageous to the electrode materials
7   [48].
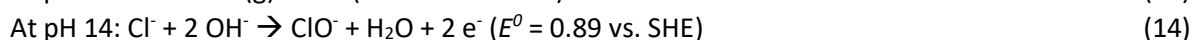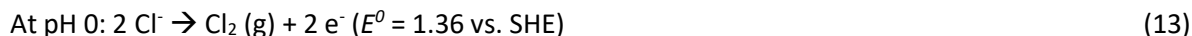
8   At pH 0: $2\ Cl^- \rightarrow Cl_2\ (g) + 2\ e^-$ (E^0 = 1.36 vs. SHE)   (13)
9   At pH 14: $Cl^- + 2\ OH^- \rightarrow ClO^- + H_2O + 2\ e^-$ (E^0 = 0.89 vs. SHE)   (14)
10   With E^0 the redox potential of the half reaction.

11   The OER is thermodynamically favored over the ClER due to its lower redox potential OER (1.23 V <
12   1.36 V vs. SHE at pH 0 [10]). Bennet already noticed in 1980 that unbuffered seawater splitting would
13   deliver mostly Cl_2 gas at realistic larger current densities. He explained this by the better kinetics of
14   the ClER. The ClER involves only two instead of four electrons, leading to smaller required
15   overpotentials. He pointed out that this effect could be avoided by using inconveniently low (< 1
16   $mA.cm^{-2}$) or very high current densities (several thousand $mA.cm^{-2}$) [105]. Note furthermore that Br^-
17   oxidation is even thermodynamically favored, but due to its low concentration (289 times lower than
18   Cl^-), it will not be considered further [10].

19   The Pourbaix diagram (Fig. 3) shows that the ClER can be avoided by operating at higher pH. Dionigi
20   *et al.* (2016) proposed a pH-value above 7.5 as a criterion for more selective O_2 evolution [47].
21   Without the addition of strong acids or bases, the pH of natural seawater is around 8 [29].
22   Nonetheless, in typical liquid-based ECs, a tremendous decrease in the local pH of 5-9 pH units is
23   observed at the anode for high current densities [11,106]. Buffers are hence necessary, despite the
24   original occurrence of borate and carbonate [10] (see Table 1). On the other hand, too high pH values
25   should also be avoided, due to safety constraints [7], faster degradation of the cell components and
26   ClO^- formation [47]. The latter can be suppressed by applying overpotentials lower than 0.48 V (Fig.
27   3). Since the pH dependence of the OER and the evolution of ClO^- are similar, this second criterion is
28   valid for all pH values above 7.5 [47].
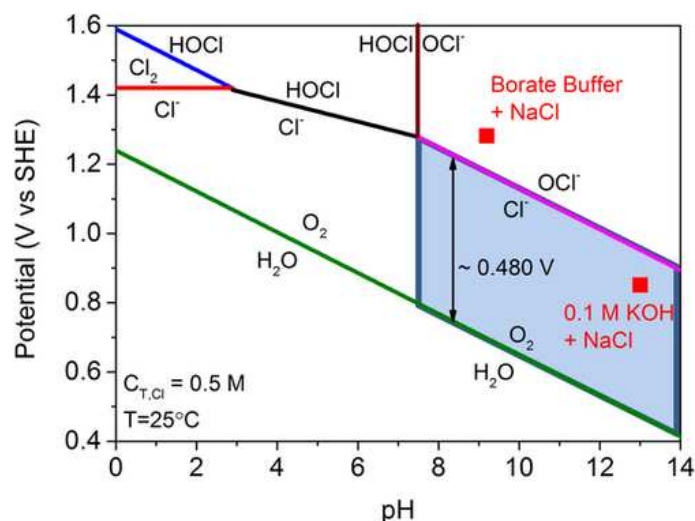
29
30   Figure 3: Pourbaix diagram containing oxygen and Cl^- redox reactions. The light blue area demarcates the OER selective
31   region for a Cl^- concentration of 0.5 M and a temperature (T) of 25°C. Reproduced with permission from Ref. [47]. Copyright
32   2016, Wiley-VCH Verlag GmbH.

To be less reliant on the reaction conditions, more robust selective solutions have been proposed [62,107–113]. One interesting strategy is the repulsion of negatively charged Cl^- species. This can be achieved using manganese based electrocatalysts. Their OER selectivity in 0.5 M NaCl solutions (simulated seawater) is very well documented for different pH values (pH 1-10) with all examples showing efficiencies exceeding 90% [62,108,109,112,114]. Another important recent example is the application of an *in situ* generated polyanion-rich passivating layer by Kuang *et al.* (2019). Next to the passivating layer, their multilayer anode contains a NiFe electrocatalyst layer attached to a NiS_x layer on porous Ni foam. This setup allowed operating at industrially required current densities (0.4-1 $A.cm^{-2}$) over 1000h. The polyatomic sulfate- and carbonate-rich passivating layers led to excellent corrosion resistance and were able to effectively repel Cl^- [46]. In order to repel the negatively charged Cl^-, the use of cation exchange membranes is often suggested (*e.g.* Nafion®)[115]. Unfortunately, these solutions suffer from membrane-related issues (see 3.5.1). Other solutions focus on the preliminary removal of Cl^- with *e.g.* a settling tank filled with an aqueous NaOH solution [116]. Finally, another interesting approach is the use of seawater vapor instead of liquid seawater (Fig. 4a). This was suggested by Spurgeon and co-workers (2016) [117]. The vapor itself contains far less ions and is sufficiently humid to maintain relatively high current densities. Coupled to photovoltaics (PV), stable STH efficiencies of about 6% were demonstrated for more than 50h at a relative humidity (RH) of 80%. In contrast, the liquid seawater equivalent lost more than 92% of its activity over this period (Fig. 4b). The performance was moreover only minimally affected by RH fluctuations as long as the relative humidity exceeded 30%. However, severe HER selectivity issues occur in these systems. Spurgeon's researchers encountered only low Faradaic efficiencies for the HER in the order of 60%. This was explained by O_2 crossover and its competing reduction reaction. A thicker membrane was hence suggested to suppress gas crossover [117].
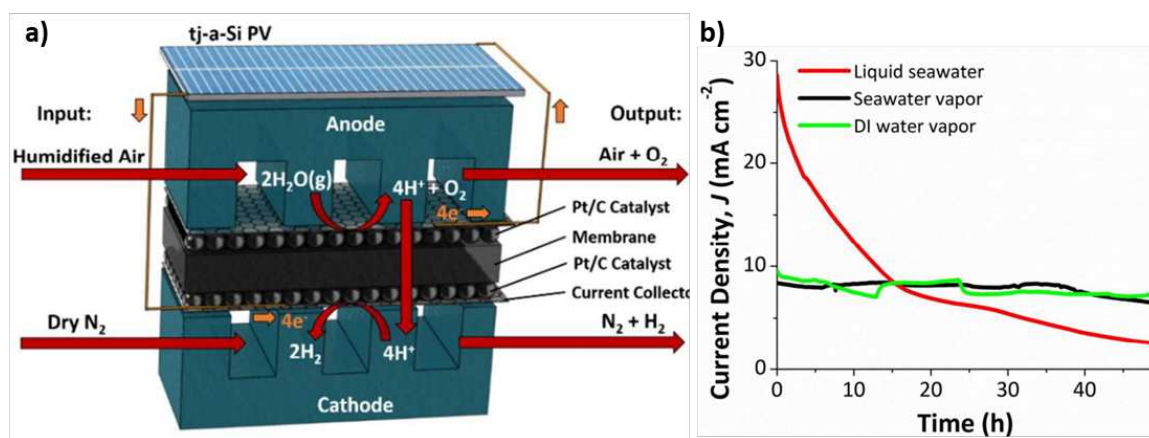
Figure 4: a) Spurgeon's seawater vapor setup. Electrical energy is delivered by triple junction amorphous Si (tj-a-Si) PV. The potential of this method is displayed in b) showing a stable current density for seawater vapor (black) and deionized vapor (DI, green) compared to that of liquid seawater (red). Current densities are measured at an applied voltage of 1.6 V, using a 80% RH vapor stream at 20 sccm for the anode and dry N_2 at 10 sccm for the cathode. Reproduced from Ref. [117] with permission from The Royal Society of Chemistry.

3.2.2 Photocatalysis and PEC seawater splitting

In contrast to electrolysis, several studies indicate that photocatalytic seawater splitting does not seem to suffer as much from Cl_2 evolution compared to electrolysis. Pioneers Ji *et al.* (2007) explored the role of salts in seawater, but never detected any formation of Cl_2 in their photocatalytic test systems (*i.e.* $La_2Ti_2O_7$ under UV light and CdS/TiO_2 under visible light (VIS)) [75]. Note that the VBs of these photocatalysts are theoretically suitable for Cl^- oxidation [40]. It was measured that the overall pH only decreased slightly from 8.5 to 8.3 [75]. Besides, it is not expected to have large local differences since both the oxidation and the reduction occurs at the same catalyst surface [32]. This

is a strong asset compared to electrolysis where pH changes are observed up to 9 pH units near the electrode surface [11]. Also, in other photocatalytic studies no chlorine production was reported, explaining it by the possible back reduction of the Cl° radical by an e^-_{CB} [77,80,118]. Guan *et al.* (2018) observed only a small amount of free chlorine (dissolved Cl_2, HClO and ClO^-) of ~0.1 mg.L^{-1} [49]. This value was negligible compared to the formed amounts of H_2 and O_2. The latter were generated in an approximately ideal 2:1 ratio. This may imply that the ClER is an intermediate reaction. Also, the role of light irradiation may not be underestimated. Cl_2 can react further with water to HClO (eq. 15) which is easily decomposed to protons, oxygen gas and Cl^- under illumination (eq. 16) [99].

$$Cl_2 + H_2O \rightarrow H^+ + Cl^- + HClO \tag{15}$$
$$2\ HClO + h.v \rightarrow 2\ H^+ + 2\ Cl^- + O_2 \tag{16}$$

With h Planck's constant (6.63×10^{-34} J.s) and v the incident light frequency.

Cooper *et al.* (2007) quantified the half-life of HClO/ClO^- under conventional sunlight irradiation as 0.28h in pure water at pH 7. This value even decreases for lower pH values [119]. Besides, Cl_2 itself can also be decomposed under illumination, giving photocatalytic technology a strong benefit over electrolysis [120]. Low-energy UV-A light already enables Cl_2 photolysis. Finally, an additional reason that helps avoiding Cl_2 evolution is the fact that many photocatalysts, such as TiO_2, have a point of zero charge below the average pH of seawater (7.5-8.4) [121]. Consequently, their surface is negatively charged which leads to Cl^- repulsion. On the other hand it means that for some materials Cl^- oxidation is technically possible, depending on their valence band position [85]. For example, Maeda *et al.* (2009) attributed the small quantity of evolved oxygen from seawater for their $(Ga_{1-x}Zn_x)(N_{1-x}O_x)$ photocatalysts to the competition with chloride oxidation [122]. However, only very small amounts of ClO^- were observed after the reaction, compared to the total Cl^- concentration. This might again indicate that the Cl species continue to react further, which should be confirmed by on-line measurements in future research.

Also in the case of PEC seawater splitting, Ji *et al.* (2007) did not detect Cl_2 evolution [75]. Conversely, Cl_2 evolution may actually increase the STH efficiency [94,95], since Cl^- can act as a hole scavenger, thus reducing the recombination rate [68]. Especially in the case of WO_3 photoanodes, Cl_2 evolution is interesting. In several studies, the ClER is used to surpass the slow kinetics of the OER due to the intrinsic properties and morphology of WO_3 [123]. Additionally, if oxygen bubbles are evolved, these could also fill the pores of the WO_3 photoelectrodes, leading to lower currents. This issue is less important for Cl_2 evolution because of its higher solubility in water [95]. Another advantage for separated WO_3 anodes is the local acidification caused by the disproportionation of Cl_2 (eq. 15). WO_3 is most stable in acidic environments [26]. Shi *et al.* (2017) obtained Faradaic efficiencies for the ClER of 56%, using porous WO_3 in 0.5 M NaCl solutions. The remaining holes were likely largely consumed in the formation of HClO. Their WO_3 film photoanode yielded a photocurrent density of 1.95 mA.cm^{-2} which was stable for 3h under 1 sun AM 1.5G solar radiation (100 mW.cm^{-2}) and at an applied potential of 1.23 V vs. RHE (Reversible Hydrogen Electrode) [94]. Recently, Jadwiszczak *et al.* (2020) could even achieve higher photocurrent densities in seawater using lower overpotentials. When anodic potentials of 0.95 V vs. RHE were applied, their nanostructured WO_3 photoanodes yielded currents exceeding 4.5 mA.cm^{-2} [95]. Yet, extra precautions should be made to monitor and take care of the formed toxic Cl_2. Possibilities to remove Cl_2 from water include evaporation, adsorption on activated coal or chemical neutralization with ascorbic acid [124]. As in the case of pure photocatalysis, due to the presence of light, Cl_2, HClO and ClO^- will also be degraded [119].

1 Finally, a possible method of avoiding Cl issues could be to translate Spurgeon's seawater vapor
2 approach to a PEC setup [117]. This can be done using gas-phase PEC cells (Fig. 5), based on the initial
3 concept of Seger & Kamat (2009) [125] and recently adapted towards hydrogen recovery from
4 polluted humid air by Van Hal *et al.* (2017). Although O_2 crossover losses have been recorded, the
5 design offers the opportunity to effectively work with vapor streams [126]. Unfortunately, actual PEC
6 studies using seawater vapor are still lacking to date, but could present a highly interesting research
7 opportunity.

8
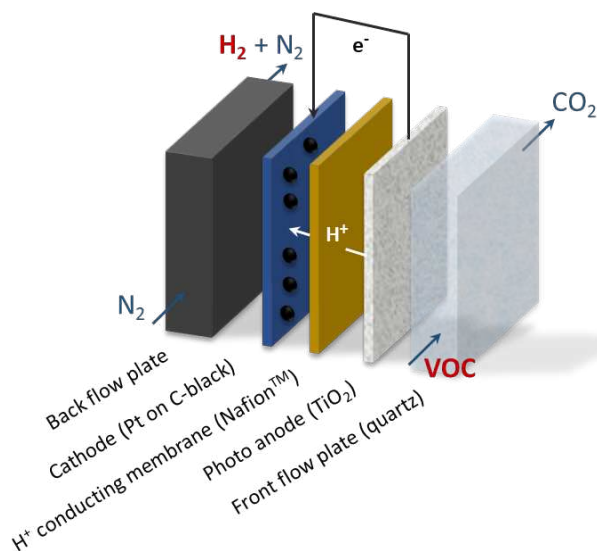
9
10 Figure 5: Gas phase PEC cell based on all solid design. Instead of a volatile organic compound (VOC) stream, a seawater
11 vapor stream could be introduced. Reproduced with permission from Ref. [126]. Copyright 2017, Wiley-VCH Verlag GmbH.

3.3 Catalyst stability
13 Next to the activity and selectivity, the stability in seawater is a crucial parameter. Important aspects
14 including corrosion, scaling, biofouling and flocculation will be discussed.

3.3.1 Electrolysis
16 Apart from the formation of Cl_2 and ClO^-, Cl^- can also cause severe corrosion of the electrodes. This
17 happens via the metal chloride-hydroxide mechanism (eq. 17-19). It consists of the Cl^- adsorption due
18 to surface polarization, which can lead to dissolution of the metal. After this, the chloride is often
19 converted to a hydroxide [46].

20 $M + Cl^- \rightarrow MCl\ (ads) + e^-$ (17)
21 $MCl\ (ads) + x\text{-}1\ Cl^- \rightarrow MCl_x^-\ (aq)$ (18)
22 $MCl_x^-\ (aq) + x\text{-}1\ OH^- \rightarrow M(OH)_x\ (s) + x\ Cl^-$ (19)

23 Corrosion in general is considered as one of the major issues of seawater electrolysis, resulting in
24 lowered yields [11]. Also for OER selective anodes such as NiFe-LDH (Layered Double Hydroxides)
25 [47], Co-borate [28] and Co-phosphate [28,127] severe corrosion on the long term is observed. It is
26 even noticed for noble metal (*e.g.* Ru) containing electrocatalysts [128]. Important for corrosion
27 processes is the dramatic pH change (up to 9 pH units in slightly buffered seawater) at the anode
28 [11]. For example, when efficient H^+ acceptors are lacking, the electrocatalyst will act as a base
29 resulting in H^+ induced corrosion [127]. Therefore, proper control over the reaction medium [117]
30 and additional modifications such as passivating layers [46] are needed in order to increase the
31 corrosion resistance. Dai's polyatomic sulfate- and carbonate- rich passivating layers are a good
32 example that lead to superior corrosion resistance [46]. Cl_2 can also cause corrosion at the cathode

due to gas crossover [129]. To prevent this, controlling the pressure gradient is key. Thicker membranes are advisable, although this will be a trade-off with the conductivity [11]. Another option is alloying the Pt or Ni cathodes with transition metals (Cr, Fe, Co and Mo) [130]. For instance, PtMo alloys on a Ti mesh lose less than 10% of their activity in seawater over 172h of operation [51]. Finally, also Spurgeon's seawater vapor approach could be helpful (see 3.2.1 and Fig. 4b).

Secondly, a tremendous pH increase can occur at the cathode when protons are rapidly consumed. This leads to very alkaline conditions. Cations such as Mg^{2+} and Ca^{2+} may hence precipitate as hydroxides [131]. This precipitation on the electrodes, called inorganic scaling, already begins at pH ≥ ~9.5 [132]. Consequently, the active sites of the cathode get blocked. Current density losses of more than 50% after 24h have been reported because of this phenomenon [131]. Proposed solutions are often based on the use of perm-selective overlayers. These block the impurities and still allow transfer of reagents and products [133]. In 2017, Ma *et al.* suggested a graphitic shell around a CoMoP electrocatalyst (Fig. 6a). By using this shell, effective protection against etching, agglomeration and blocking of active sites could be obtained (Fig. 6b). However, close attention should be paid to possible mass transport issues [57].
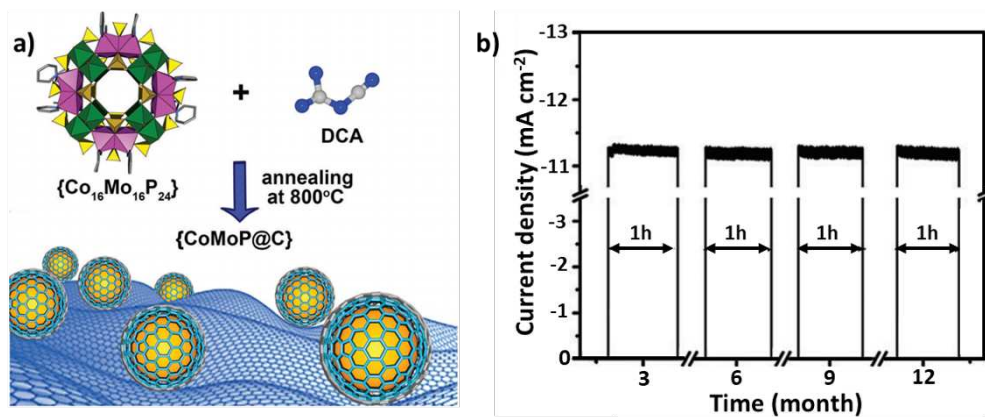
Figure 6: a) Configuration of Ma's CoMoP@C electrocatalyst for which the N-doped carbon shell is formed from dicyandiamide. b) Current density vs. time plots for CoMoP@C under a static overpotential of 180 mV during 1h for 12 months with an interval of 3 months. Reproduced from Ref. [57] with permission from The Royal Society of Chemistry.

Finally, active site blocking can also originate from organic matter, if no seawater pre-treatment is applied [134]. Next to active site blocking, biofouling can locally attack metallic materials and consequently cause crevice corrosion [135]. Alternatively, it is stated that electrochemical reactions can generate ROS at sufficiently large overpotentials [48]. Important examples of these ROS are the hydroxyl radical at the anode and the superoxide anion radical at the cathode [32], that can oxidize organic matter. Also chlorine species could play that role bringing them back to the Cl⁻ state [48]. It should be noted that the occurrence of ROS and Cl_2 is far less likely at the cathode [136]. Esposito's group developed impurity tolerant membrane coated electrocatalysts for the cathode. These catalysts are based on ultrathin layers of SiO_x coated onto Pt films. The SiO_x overlayers act here as poison resistant nanomembranes which still easily allow the H^+/H_2 transport [137]. Nevertheless, further research for the effect of impurities in ECs and impurity resistant materials could be very advantageous to the community [11].

3.3.2   Photocatalysis and PEC seawater splitting

As mentioned previously, local pH fluctuation-induced corrosion is not considered a significant problem for photocatalysts. Reported pH changes are in the order of 0.1-1 pH unit [75,99] *vs*. 5-9 units for electrolytic seawater splitting [11]. The most common semiconductor photocatalyst, TiO_2, is also a chemically stable oxide [138]. Its outstanding chemical stability originates from the fact that O^{2-} is a hard nucleophile [32]. Unfortunately, this also results in a large band gap since the VB consists of the low energy O 2p orbitals [32]. On the other hand, small band gap photocatalysts such as metal chalcogenides [40], (oxy)nitrides [139,140] and oxysulfides [141] suffer from poor stability. In general, corrosion, and photo-corrosion in particular (which obviously does not occur in ECs), are major issues here [40]. Cheng *et al.* (2016) observed for example performance losses of more than 95% for orthorhombic Ag_8SnS_6 in a 0.5 M NaCl solution due to its poor stability. To solve this, the use of sacrificial agents such as Na_2S and K_2SO_3 is suggested [100]. Further, the application of co-catalysts could also enhance the corrosion resistance. MoS_2 seems very promising to inhibit photo-corrosion and can improve charge separation and light absorption (absorbance edge around 1040 nm) [142]. Another promising strategy to broaden the activity spectrum of oxide photocatalysts is the deposition of plasmonic nanoparticles (Pt [76], Pd [143], Ag [144,145] and Au [36,146–149]). These possess the optical property of (Localized) Surface Plasmon Resonance ((L)SPR) which can enable the utilization of visible light [150]. These metal particles function additionally as electron sinks under UV illumination, thereby lowering the likelihood of recombination [151]. Especially Ag seems promising due to its lower cost and strong SPR response.   Unfortunately, also these noble metals quickly aggregate and oxidize in saline media, and should thus be stabilized. As a solution, work by the Verbruggen group reports on the effect of a stabilizing polyelectrolyte shell. By applying the Layer-by-Layer (LbL) technique, a homogeneous capping layer was deposited around the Ag nanoparticles with thickness control up to the sub-nanometer level (Fig. 7a) [145]. The thin shell ensured the plasmonic effect was not compromised, while superior stability of plasmonic Ag nanoparticles could be achieved, which was demonstrated by adding a 1 M NaCl solution to the particle suspension (Fig. 7b). An alternative stabilizing technique is the full embedment of the plasmonic particles in the photocatalyst layer itself [146].
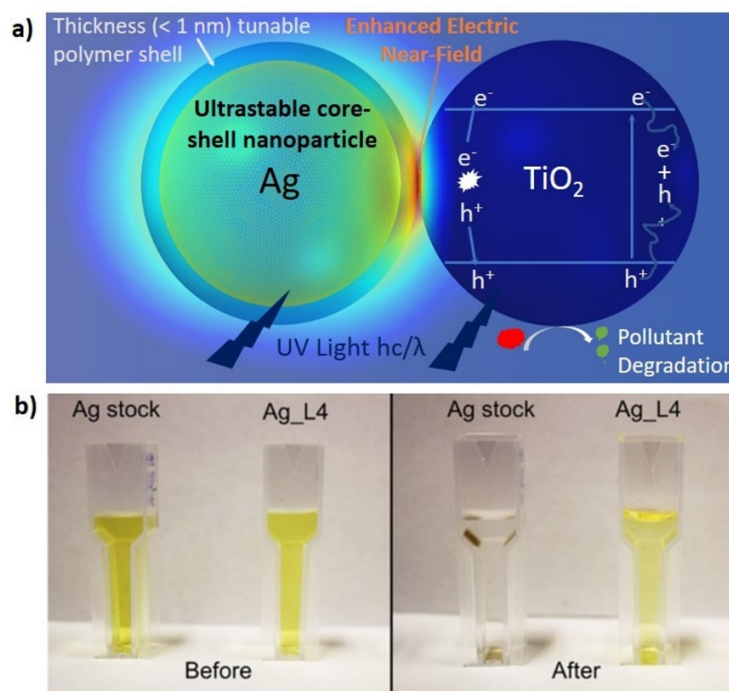
The effect of scaling due to inorganic ions is ambiguous. Ichikawa (1997) reported in the first seawater splitting study using photocatalysts that the surface of a thin anatase TiO_2 film remained clean and free from deposits. He considered this as a strong advantage over seawater electrolysis [90]. Still, Ji *et al.* (2007) tested the effect of NaCl, $MgCl_2$, $MgSO_4$, $CaSO_4$, K_2SO_4, K_2CO_3 and $MgBr_2$ in simulated seawater. It was revealed that all the dissolved electrolytes decreased the H_2 formation rates compared to pure water, except K_2SO_4. $MgCl_2$ appeared to be the most detrimental salt. A solution containing *ca.* 74% and 15% of the Mg^{2+} and Cl^- content of natural seawater, respectively, resulted in the lowest activity (decreased rates with a factor of ~2 compared to pure water). It was also demonstrated that simulated seawater without $MgCl_2$ clearly outperformed seawater containing all seven salts. Hereby, Mg^{2+} was exposed as the main culprit [75]. Hence, it can be beneficial to selectively exclude this ion. Despite membrane related issues (see 3.5.2), polyelectrolyte multilayer membrane consisting of polyvinyl alcohol and -sulfate can offer a solution. These reject 98% of Mg^{2+} from seawater [152].

Anions are also further investigated for their influence on the photocatalytic activity. Although Krivec *et al.* (2014) pointed out the detrimental effect of Cl^- active site blocking on TiO_2 [153], the effect of anions can actually be beneficial. It has been shown that carbonates facilitate O_2 desorption on ZrO_2 photocatalysts via a carbonate radical pathway. Back reactions between H_2 and O_2 are consequently suppressed [154]. In addition, small amounts of Cl^- are known to be effective against peroxo-forming side reactions [155]. These unwanted side reactions can lead to significant activity decreases [156]. Also, the usage of stabilizing co-catalysts such as Co oxides is found to be effective against the peroxo formation on WO_3. Peroxo compounds are strong poisons for C_3N_4 photocatalysts as well. Therefore, Liu *et al*. (2015) introduced extra stabilizing carbon dot (CD) co-catalysts. These CDs degrade peroxo species, leading to a long-term stability of at least 200 days[66]. Zhu *et al.* (2019) showed that these CDs allow the distraction of various ionic components in seawater. Secondly, they give rise to more efficient charge separation in CDs/CdS composites, resulting in 265 times higher H_2 evolution rates than for unmodified CdS [86].

Finally, biofouling has never been reported as a severe issue, to the best of our knowledge. This could be explained by the fact that photocatalysts are very prone to generate ROS. ROS can effectively degrade organic matter [32]. Therefore, TiO_2 photocatalysts are often applied on different kinds of substrates to decompose organic fouling [146,157–159]. This is an advantage over compartmentalized cells such as ECs and PECCs. On the other hand, an advantage of such cells over plain photocatalysts is the lack of flocculation effects: In photocatalyst slurries, flocculation can occur due to the presence of salts. The ions may remove the electrostatic repulsion. Sakurai *et al.* (2018) noticed that the resulting agglomeration and decrease in active surface area led to halved H_2 yields for granular Pt/TiO_2. This flocculation behavior is, at least in part, reversible. For Sakurai's system, enhanced stirring or a Na^+ decrease was already helpful [76].

For PEC seawater splitting, the situation depends strongly on the materials used. For the OER, chemically stable photocatalysts, sometimes modified with co-catalysts, are advisable. Luo *et al.* (2011) showed that unmodified Mo-doped $BiVO_4$ photoanodes in seawater underwent photocurrent decreases from 18 mA.cm^{-2} to 12 mA.cm^{-2} after 270 min under 1 sun illumination. After modification with RhO_2, the photocurrent densities were stabilized around 16.7 mA.cm^{-2} [99]. At the cathode, similar problems as for ECs can be observed. Ayyub *et al.* (2018) explained performance decreases by flaky $Mg(OH)_2$ layers shown by Scanning Electron Microscopy (SEM, Fig. 8a-c) and Energy Dispersive X-ray analysis (EDX, Fig. 8d-f). The adverse blocking effect of formed $Cu(OH)_2$ was suggested as well. This Cu hydroxide might be formed from the Cu_2O-CuO-Ni_xP_y electrodes [85]. To stabilize the cathode, opportunities lie in the use of chemically stable oxides as a protecting layer. Kawde *et al.* (2018) showed the potential of TiO_2 protection layers for p-Si photoanodes with NiO_x. Without the extra layer, the silicon would oxidize rapidly, but no declined activity was observed during a 5h test with the protected photoanodes. Excellent photocurrent densities of 10 and 20 mA.cm^{-2} could moreover be achieved for applied potentials of 0.7 V and 0.9 V *vs*. RHE using this system [89].
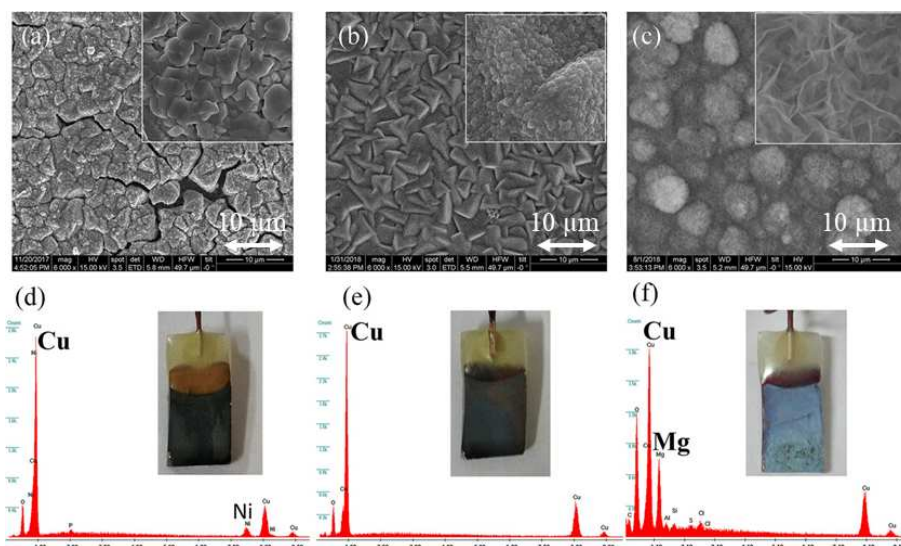
Figure 8: SEM of Cu_2O-CuO-Ni_xP_y photocathode a) before and after 1 sun AM1.5G illumination during 3h in b) distilled water and c) seawater. EDX of photocathode d) before and after the illumination in e) distilled water and f) seawater. The insets display the color of the photocathode. Note the blue-white hydroxide layer for the seawater cathode. Reproduced with permission from Ref. [85]. Copyright 2017, Wiley-VCH Verlag GmbH.

As a final remark, it is even stated in several studies that salts in seawater could act as an ideal electrolyte if corrosion and scaling issues are solved [70,92,160]. Important parameters are composition, concentration and ionic strength [92]. Concentrating seawater is therefore suggested to increase the ionic conductivity, potentially leading to lower ohmic losses [160]. Even RO waste streams could be useful. Hence, also coastal environmental pollution could be avoided [70].

3.4 Catalyst sustainability

Another factor of paramount importance is the sustainability of the used catalysts. This determines factors like the eventual H_2 cost and upscaling possibilities. The following paragraphs will therefore discuss the most commonly used materials and present some sustainable alternatives.
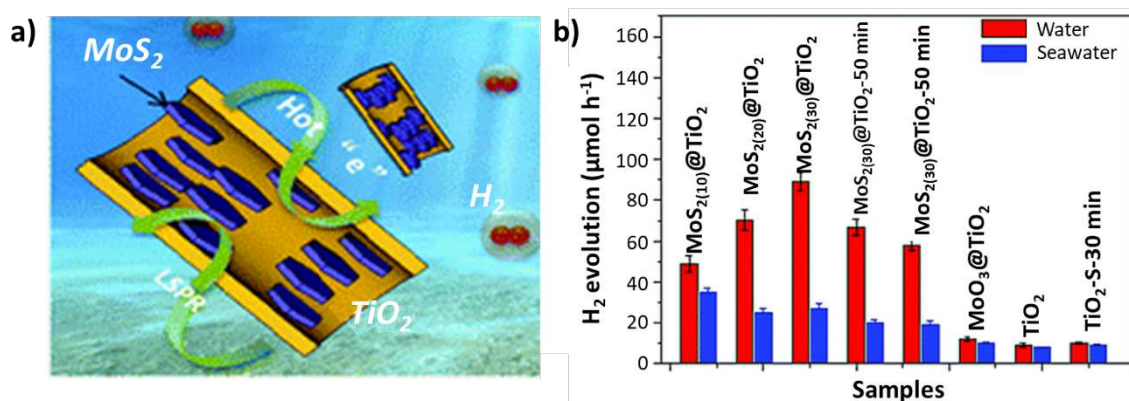
3.4.1   Electrolysis

As mentioned before, PGMs belong to the best performing electrode materials. Only under very alkaline conditions (30% KOH in water), first row transition metals and their oxides display reasonably high activities for the HER and OER [7]. Certainly for PEMECs, Pt- and Ir-based catalysts are considered as the benchmarks [52].

Unfortunately, rational design strategies that have been applied to replace PGMs in studies involving pure water cannot be directly extrapolated to seawater environments. An example is Trasatti's volcano plot that revealed sustainable alternative materials for Pt. This plot captures the relation between the HER exchange current density and the metal-hydrogen bond strength [161]. By combining elements from opposite sides of the plot, promising composite materials could be generated. For example, Lu *et al.* (2015) combined Cu surfaces with Ti dopants, yielding materials with a Pt-like H-binding energy. This strategy has yielded remarkably stably performing structures for pure water splitting. $Cu_{95}Ti_5$ exhibited even twice the activity of state-of-the-art Pt/C electrocatalysts [162]. However, CuTi composites appear to suffer from pitting corrosion in seawater, and are thus a lot less promising in that context [163]. Still, after proving to be promising alternatives to PGM HER electrocatalysts in pure water [164,165], several abundant transition metals such as Co [58], Fe [60] and Ni [52], as well as transition metal phosphides (*e.g.* CoMoP [57]) have found their way into seawater research in recent years. The same goes for OER materials, although these still strongly suffer from corrosion [47,127].

3.4.2   Photocatalysis and PEC seawater splitting

Various oxides based on earth-abundant elements are often applied as photocatalysts. Yet, possible sustainability issues may occur due to use of very specific oxides and co-catalysts. The highest activities are often brought about by components containing rare earth metals like Ta. Replacing such metals by inexpensive, abundant fourth-period transition metals would be desirable [65]. Since many oxide semiconductors exhibit a low solar activity, co-catalysts are regularly added which impacts the catalyst's sustainability. For instance, rare noble metals like Pt [76], Pd [143], Ag [144] and Au [146] perform very well since they improve both the charge separation as the solar light absorption due to plasmonic effects. To investigate the benefits of the plasmonic effect with earth-abundant components, Guo *et al.* (2018) synthesized nonmetal plasmonic $MoS_2@TiO_2$ heterostructures (Fig. 9a). In pure water, these photocatalysts achieved high H_2 yields of 181 μmol.h^{-1}.cm^{-2} under 1 sun AM 1.5G illumination. This value was 8 times higher compared to bare TiO_2, but decreased by a factor 2-3 in seawater (Fig. 9b), showing the importance of stability [73]. Other sustainable promotors for improving the performance of large band gap oxides in seawater research include CuO [74], NiO [166] and NiS [82].

Figure 9: a) Representation of non-noble plasmonic MoS_2/TiO_2 heterostructures. b) H_2 evolution rates for several MoS_2/TiO_2 heterostructures with different geometric areas in pure (red) and seawater (blue). The values for pristine and sulfurated TiO_2, and oxidized Mo on TiO_2 are about 8 times lower than for MoS_2/TiO_2. Reproduced from Ref. [73] with permission from The Royal Society of Chemistry.

Next, non-oxide earth-abundant small band gap photocatalysts are studied extensively. For example, Qiu *et al.* (2017) revealed the potential of $Cd_{0.25}Zn_{0.75}Se/CoP$, displaying an interestingly stable H_2 formation rate of 36.6 mmol.h^{-1}.g^{-1} in seawater [87]. Equally interesting are sustainable carbon-based materials. In 2015, Liu *et al.* introduced the use of low-cost, earth-abundant and environmentally friendly C_3N_4 (E_g = 2.7 eV) in seawater research [66]. Speltini *et al.* (2018) further improved g-C_3N_4's activity by a facile HNO_3 refluxing pretreatment, increasing the surface area, electron transport and reduction capacity. The subsequent oxidized g-C_3N_4 performed 5 times better than TiO_2 in seawater splitting due to its smaller band gap and more beneficial position of the CB [167]. However, Pt co-catalysts are often applied to enhance the H_2 evolution, although alternatives such pyridine cobaloxime based co-catalysts are recently appearing as well [168]. In addition, g-C_3N_4 is often combined with other abundant photocatalysts as well [68,93,98]. For example, WS_2/TiO_2/g-C_3N_4 heterojunction composites showed high HER rates of 4.56 mmol.h^{-1}.g^{-1} for 5h [68]. Another interesting class of small band gap materials is based on carbonaceous polymers. Liu *et al.* (2018) developed electron donor-acceptor covalent organic polymers (COP) using 1,3,6,8-tetrabromopyrene (donor) and 3,8-dibromophenantroline (acceptor) with a band gap of 1.76-1.84 eV [169]. Ultra-stable structures were attained by a Ni catalyzed Yamamoto-type Ullmans cross-coupling reaction which allowed the use of seawater. To exclude any PGM co-catalysts, corrosion resistant carbon encapsulated Ni_2P substitutes were recently introduced. These sustainably modified COP photocatalysts achieved stable 2.5 mmol H_2 h^{-1}.g^{-1} evolution over half-a-month of intermittent testing [170]. Finally, also 2 dimensional covalent organic frameworks (COF) have been studied in a seawater context, but currently suffer much from Mg^{2+} chelation, yielding less active structures [171].

For PEC cells, the use of earth-abundant materials for the photoanode in seawater is quite well documented [69,88,94,95,97–99,156,172]. Yet, similar activity issues arise as for pure photocatalysts. On the cathode side, Pt is usually used [173]. In order to replace it, p-Si as a photoactive substrate with deposited HER electrocatalysts (*e.g.* Mo sulfides) has been suggested [174]. However, Si electrodes suffer from their poor stability. The same is observed for Cu_2O (with an ideal E_g of about 2 eV) [175]. Hence, the use of abundant co-catalysts like Ni [175] and protecting layers consisting of *e.g.* ZnO and TiO_2 is studied [176]. An alternative is the use of Co-based materials [88,177]. Patel *et al.* (2017) applied porous and semi-transparent Co_3O_4 photocathodes for achieving high current densities of 25 mA.cm^{-2} under 1 sun illumination and a bias of 0.83 *vs*. RHE. Due to the dual band gap character of the porous Co_3O_4 (E_g = 1.5 and 2.3 eV), high photo conversion efficiencies of 9% and 2% could be obtained for UV and visible light wavelengths, respectively [88].

3.5 Use of membranes

Although the catalyst is considered to be the crucial component in all systems, the use of membranes is simply often required in ECs and PEC cells. They may moreover serve to overcome some of the difficulties when working in seawater, as mentioned before (see 3.2.1). Membranes are known to be affected by ions and impurities as well [178].

3.5.1 Electrolysis

Membranes are prominently present in PEMECs and AEMECs where they guarantee the ion-selective transfer of protons and hydroxide anions, respectively. This also leads to physical separation of the reaction products, increasing the final hydrogen yields [179]. The most common membranes in PEMECs are based on Nafion® [136]. These humid sulfonated tetrafluoroethylene-based polymers benefit from their high proton conductivity, good thermal properties and chemical stability in pure water. Unfortunately, it increases the cost of the device significantly [180]. Their lifetime is severely compromised in seawater due to blocking by Na^+, Mg^{2+} and Ca^{2+} which decreases the membrane performance [181]. This resulted in high water purity requirements for PEMECs (18 MΩ.cm) making their use in seawater unfeasible. In AEMECs on the other hand, similar issues are observed due to the anions present (Cl^-, Br^-, SO_4^{2-} …) [10]. Boettcher's group pointed out that anion exchange membranes are still significantly less stable and active than their more developed cation equivalents [182]. Dresp *et al.* showed a first working membrane-based AEMEC on artificial seawater in 2018 [29]. They used a NiFe LDH anode and a Tokuyama A201 AEM. After addition of 0.5 M NaCl to several KOH solutions (0.1-1.0 M), a remarkable current density decrease was noticed. This decrease could only be related to Cl^- blocking of the membrane, as no adverse effect of NaCl on the catalysts and electrodes was observed [29].

An alternative approach is the use of a Zirfon diaphragm due to its robustness, but these systems suffer from their lack of functional exchange groups. This results in a low ion conductivity [183]. The use of a membrane also generates a pH gradient between the electrodes. This causes an efficiency decrease since the theoretical electrolysis voltage increases. It is expected that this effect will be more significant for larger distances between the electrodes [184]. Besides, biofouling may occur as it is also observed for reverse osmosis membranes [178]. An interesting solution refers back to the seawater vapor approach of Spurgeon and co-workers (2016) [117]. These systems exclude the majority of ions, as mentioned earlier in 3.2.1. The ultimate solution, however, for all the membrane-related problems mentioned thus far, is to completely remove it from the cell design. In that regard Esposito's group introduced in 2018 floating membraneless PV-electrolyzers with buoyancy-driven product separation (Fig. 10a) [48]. These electrolyzers contain mesh electrodes with asymmetrically deposited electrocatalysts (Fig. 10b). Using this system, product crossover rates could drop to only 1% without the use of any membrane.
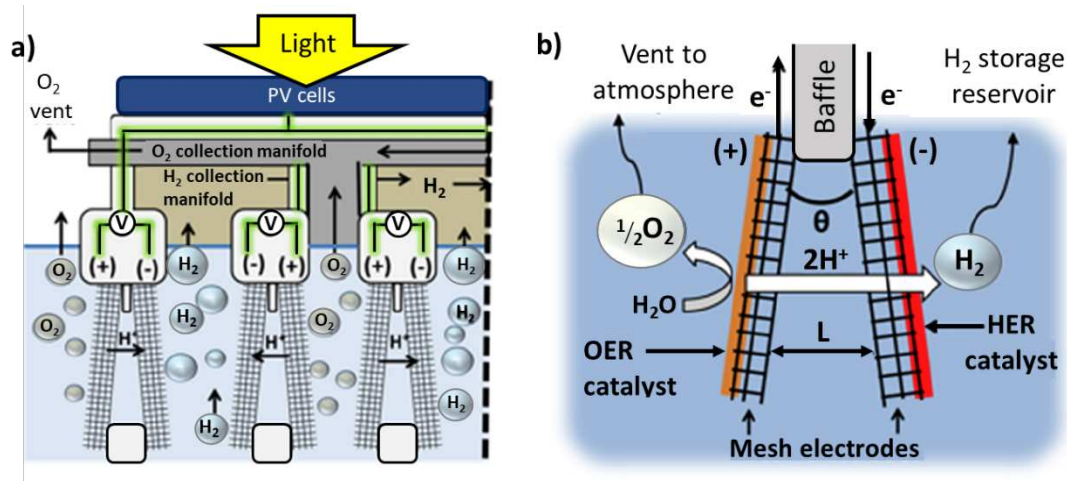
Figure 10: a) Schematic representation of a membraneless electrode setup. The required voltage is supplied by PV cells. b) Detail of the setup in (a). The mesh electrodes with asymmetrically outward deposited electrocatalysts are placed under a well-defined angle (θ), separated by certain length (L). The gas bubbles will float upwards after they have grown sufficiently in size. Reproduced with permission from Ref. [48], Copyright (2018), with permission from Elsevier.

3.5.2   Photocatalysis and PEC seawater splitting

Another way of surpassing membrane related issues is the use of photocatalysis, as pointed out by Dresp *et al.* (2019) [10]. For pure photocatalysts, the use of membranes is not required. This has consequences for the hydrogen yield since the reaction products are not physically separated [185]. A solution to suppress the back reaction is the use of oxyhydroxide layers as an O_2 impermeable surface coating. This was successfully applied for pure water splitting by Pan *et al.* (2015) using complex perovskite-type oxynitride photocatalysts ($LaMg_xTa_{1-x}O_{1+3x}N_{2-3x}$ with x ≥ 0.33) [186]. A more established solution is the use of hole scavengers. These often lead to a higher efficiency in seawater than in pure water due to better adsorption [84,187]. The available ions may remove any electrostatic repulsions between the scavenger and the photocatalyst [84]. Another issue related to the absence of gas separation is the possibility of forming an explosive gas mixture [66]. However, several industrial techniques are already sufficiently mature to extract and separate the H_2 gas such as pressure or temperature swing adsorption [43] and electrochemical pumps [66].

Since PEC water splitting devices are similar to ECs [26], the types of membranes involved and the related issues are similar to those discussed above. Gas-phase PEC cells (see 3.2.2) might at least partially solve the fouling problems, again highlighting the potential of using seawater vapor, also in PEC cells.

3.6 Electricity requirements

The last discussed parameter is the need for electricity, since this is also an important difference between both technologies.

3.6.1   Electrolysis

Electrolysis is by nature an electricity-driven process. d'Amore-Domenech *et al.* (2019) calculated that the required electric energy for producing 1 kg H_2 (at 350 bar) amounts to 452.0 MJ if direct seawater electrolysis is applied (Fig. 11). This value is rather high, compared to the estimated 174.6 $MJ.kg^{-1}$ H_2 for low-temperature pure water electrolysis. It should also be noted that the heat delivered by the electrolyzer cannot be used for co-generation under the studied conditions (operation temperature of 15.9 °C) [188]. Possibly, energy efficiency gains may be obtained by adding more electrolytes to increase the ionic conductivity [160]. To deliver the required energy, several sustainable solutions have been explored that are available in a marine environment, *i.e.* close to the source of seawater. Potential energy sources are *e.g.* salinity and thermal gradients, wave, tidal, solar and wind energy [188].
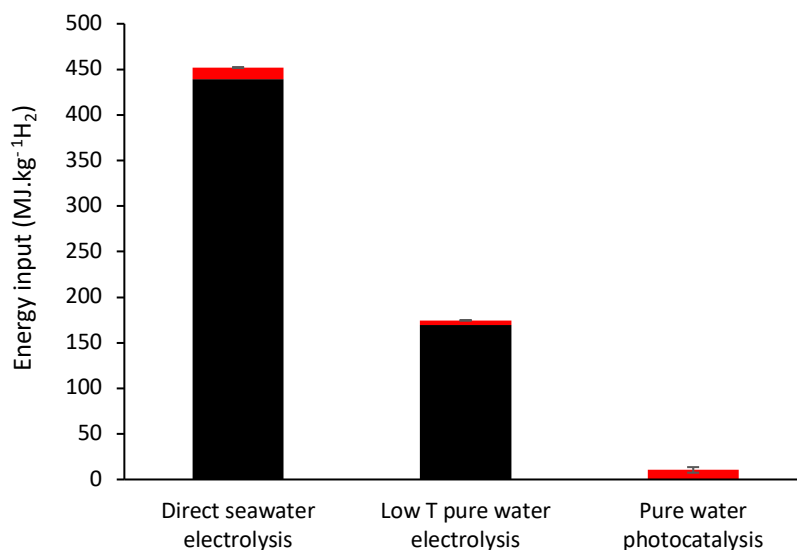
Figure 11: Comparison of energy requirements for the electrolyzer (black), and balance of plant* (BOP, red) for both electrolytic and photocatalytic water splitting systems. The results are based on the studies of d'Amore-Domenech *et al.* (2019) and Pinaud *et al.* (2013). The error bar for photocatalysis gives the average deviation for different types of photocatalytic systems (single and dual bed particle suspension, fixed panel array and tracking concentrator array). *The BOP consists of the compressor, pump and control system requirements. The replacement of the panels is not considered here. Based on the values reported in Ref. [188], Ref. [189] and Ref. [43].

3.6.2   Photocatalytic and PEC seawater splitting

One of the major advantages of photocatalysis compared to electrolysis, is the fact that no external electricity input is required, thus avoiding the associated efficiency losses [190]. PEC cells can in principle also benefit from this advantage, although often an external bias is applied to enhance the activity. Moreover, an energy input of 7-15 MJ per kg H_2 is always required for the utility systems [189]. In multiple studies several tenths of Volts are commonly applied as external bias [7]. The effect of this bias is not as straightforward, since the excess energy leads to a temperature increase of the environment. This in turn results in a lower required energy for the photocatalytic redox reactions [191]. On the other hand it again increases the recombination rate and the rate of reagent desorption as well [192]. In an early study, Raja *et al.* (2006) demonstrated that the optimal photon conversion efficiency for TiO_2 nanotubular arrays in a 3.5 wt% NaCl solution was obtained for a potential applied to the anode of 0.6 V vs. Ag|AgCl [191]. To further minimize the overpotentials,

electrocatalysts can be added [41]. Important pioneers for this were Chorkendorff and co-workers who assembled electrocatalytic Mo_3S_4 and red photon absorbing p-Si photocathodes for pure water splitting. This modification made it possible to work quite efficiently without external bias [174]. More specifically in seawater research, Kawde *et al.* (2018) implemented p-Si/TiO_2 photocathodes without external bias. These already showed to work 15 times better after the addition of NiO_x [89]. So, the possibility of working without extra electric energy input is clearly a strong advantage for these processes. Hence, Glenk and Reichelstein (2019) stated that despite their early commercial stage, they may improve the economics of renewable H_2 generation in the future [44].

4. Conclusion and outlook

In this review, photocatalytic and PEC seawater splitting are compared to seawater electrolysis. Seawater electrolysis heavily benefits from a high overall activity that is reached to date, while the efficiency of photocatalytic and PEC processes is strongly limited by their dependence on solar light. On the other hand, these technologies may appear superior when selectivity and stability in seawater are concerned. In photocatalysis, harmful Cl_2 and ClO^- formation tend to be less problematic than for electrolysis, but the actual fate of Cl-species has not yet been fully elucidated is such systems. Besides, conventional ECs suffer strongly from corrosion and inorganic scaling due to the very high local pH changes (up to 9 pH units) occurring at the electrodes. Hence, to deal with the aforementioned selectivity and stability issues, future EC research may benefit from focusing on the application of perm-selective, passivating overlayers, excluding harmful ions and other interfering components in seawater. Another promising research suggestion is the implementation of Spurgeon's seawater vapor approach for more sustainable, earth-abundant metal based electrodes. On the other hand, large pH changes are simply not observed for pure photocatalysts, where they are measured to be limited to several tenths of a pH unit. Photocatalysts are also considered more resistant toward biofouling because of the formation of reactive oxygen species. Other benefits of direct photocatalysis lie in the fact that membranes and additional electricity input are not strictly needed. This makes this young research domain still promising to achieve the DOE targets. However, in order to attain these targets, the solar light utilization capacity of current photocatalysts will need to be improved further. Therefore, research on abundant, small band gap photocatalysts in combination with sustainable co-catalysts is encouraged. However, additional stabilization methods will need to be considered to guarantee long-term performance. Finally, more optimized photocatalysts can be implemented in PEC cells. These cells suffer from several EC-like disadvantages, but benefit from the immediate separation of the evolved gases. Especially all-solid PEC designs operating on seawater vapor have been identified as a potentially promising strategy due to reduced Cl_2 formation, diminished corrosion and scaling, thus offering great new research opportunities.

Finally, while seawater electrolysis is clearly the most established technology to date, photocatalysis offers crucial advantages toward selectivity and (long term) stability that could stimulate its further development for applications on the intermediate and long term, while photoelectrochemical techniques may be able to compromise between advances in both fields.

Acknowledgements

CRediT authorship contribution statement

Fons Dingenen: Conceptualization, Investigation, Resources, Data Curation, Writing - Original Draft, Visualization, Funding acquisition

Sammy W. Verbruggen: Conceptualization, Resources, Writing – Review & Editing, Visualization, Supervision, Funding acquisition

References

[1]   International Energy Agency. World Energy Outlook 2017. Paris: 2017.

[2]   Nikolaidis P, Poullikkas A. A comparative overview of hydrogen production processes. Renew Sustain Energy Rev 2017;67:597–611. https://doi.org/10.1016/j.rser.2016.09.044.

[3]   Sobrino FH, Monroy CR, Pérez JLH. Critical analysis on hydrogen as an alternative to fossil fuels and biofuels for vehicles in Europe. Renew Sustain Energy Rev 2010;14:772–80. https://doi.org/https://doi.org/10.1016/j.rser.2009.10.021.

[4]   Dincer I, Acar C. Review and evaluation of hydrogen production methods for better sustainability. Int J Hydrogen Energy 2015;40:11094–111. https://doi.org/https://doi.org/10.1016/j.ijhydene.2014.12.035.

[5]   Fuel Cells and Hydrogen Joint Undertaking (FCH). Hydrogen Roadmap Europe - a Sustainable Pathway for the European Energy Transition. 2019. https://doi.org/10.2843/249013.

[6]   Sapountzi FM, Gracia JM, Weststrate CJ, Fredriksson HOA, Niemantsverdriet JW. Electrocatalysts for the generation of hydrogen, oxygen and synthesis gas. Prog Energy Combust Sci 2017;58:1–35. https://doi.org/https://doi.org/10.1016/j.pecs.2016.09.001.

[7]   Roger I, Shipman MA, Symes MD. Earth-abundant catalysts for electrochemical and photoelectrochemical water splitting. Nat Rev Chem 2017;1:3. https://doi.org/10.1038/s41570-016-0003.

[8]   Maeda K. Photocatalytic water splitting using semiconductor particles: History and recent developments. J Photochem Photobiol C Photochem Rev 2011;12:237–68. https://doi.org/https://doi.org/10.1016/j.jphotochemrev.2011.07.001.

[9]   Bard AJ, Fox MA. Artificial Photosynthesis: Solar Splitting of Water to Hydrogen and Oxygen. Acc Chem Res 1995;28:141–5. https://doi.org/10.1021/ar00051a007.

[10]   Dresp S, Dionigi F, Klingenhof M, Strasser P. Direct Electrolytic Splitting of Seawater: Opportunities and Challenges. ACS Energy Lett 2019;4:933–42. https://doi.org/10.1021/acsenergylett.9b00220.

[11]   Tong W, Forster M, Dionigi F, Dresp S, Sadeghi Erami R, Strasser P, et al. Electrolysis of low-grade and saline surface water. Nat Energy 2020;5:367–77. https://doi.org/10.1038/s41560-020-0550-8.

[12]   Zhang J, Hu W, Cao S, Piao L. Recent progress for hydrogen production by photocatalytic natural or simulated seawater splitting. Nano Res 2020. https://doi.org/10.1007/s12274-020-2880-z.

[13]   d'Amore-Domenech R, Santiago Ó, Leo TJ. Multicriteria analysis of seawater electrolysis technologies for green hydrogen production at sea. Renew Sustain Energy Rev 2020;133:110166. https://doi.org/https://doi.org/10.1016/j.rser.2020.110166.

[14]   Taikhao S, Incharoensakdi A, Phunpruch S. Dark fermentative hydrogen production by the unicellular halotolerant cyanobacterium Aphanothece halophytica grown in seawater. J Appl Phycol 2015;27:187–96. https://doi.org/10.1007/s10811-014-0292-8.

[15]   Cai J, Wang G, Pan G. Hydrogen production from butyrate by a marine mixed phototrophic bacterial consort. Int J Hydrogen Energy 2012;37:4057–67. https://doi.org/https://doi.org/10.1016/j.ijhydene.2011.11.101.

[16]   Kumaravel V, Abdel-Wahab A. A Short Review on Hydrogen, Biofuel, and Electricity Production Using Seawater as a Medium. Energy & Fuels 2018;32:6423–37. https://doi.org/10.1021/acs.energyfuels.8b00995.

[17] Ipsakis D, Kraia T, Marnellos GE, Ouzounidou M, Voutetakis S, Dittmeyer R, et al. An electrocatalytic membrane-assisted process for hydrogen production from H2S in Black Sea: Preliminary results. Int J Hydrogen Energy 2015;40:7530–8. https://doi.org/https://doi.org/10.1016/j.ijhydene.2014.12.017.

[18] Zou M-S, Yang R-J, Guo X-Y, Huang H-T, He J-Y, Zhang P. The preparation of Mg-based hydro-reactive materials and their reactive properties in seawater. Int J Hydrogen Energy 2011;36:6478–83. https://doi.org/https://doi.org/10.1016/j.ijhydene.2011.02.108.

[19] Fukuzumi S, Lee Y-M, Nam W. Fuel Production from Seawater and Fuel Cells Using Seawater. ChemSusChem 2017;10:4264–76. https://doi.org/10.1002/cssc.201701381.

[20] Trasatti S. Water electrolysis: Who first? J Electroanal Chem 1999;476:90–1. https://doi.org/10.1016/S0022-0728(99)00364-2.

[21] Decker F. Volta and the "pile." Electrochem Encycl 2005.

[22] Volta A. On the Electricity Excited by the Mere Contact of Conducting Substances of Different Kinds. Philos Trans R Soc London 1800;90:403–31.

[23] Seger B, Castelli IE, Vesborg PCK, Jacobsen KW, Hansen O, Chorkendorff I. 2-Photon tandem device for water splitting: comparing photocathode first versus photoanode first designs. Energy Environ Sci 2014;7:2397–413. https://doi.org/10.1039/C4EE01335B.

[24] Vincent I, Bessarabov D. Low cost hydrogen production by anion exchange membrane electrolysis: A review. Renew Sustain Energy Rev 2018;81:1690–704. https://doi.org/https://doi.org/10.1016/j.rser.2017.05.258.

[25] Laguna-Bercero MA. Recent advances in high temperature electrolysis using solid oxide fuel cells: A review. J Power Sources 2012;203:4–16. https://doi.org/https://doi.org/10.1016/j.jpowsour.2011.12.019.

[26] Bajorowicz B, Kobylański MP, Malankowska A, Mazierski P, Nadolna J, Pieczyńska A, et al. 4 - Application of metal oxide-based photocatalysis. In: Zaleska-Medynska A, editor. Met. Oxides, Elsevier; 2018, p. 211–340. https://doi.org/https://doi.org/10.1016/B978-0-12-811634-0.00004-4.

[27] Yu L, Zhu Q, Song S, McElhenny B, Wang D, Wu C, et al. Non-noble metal-nitride based electrocatalysts for high-performance alkaline seawater electrolysis. Nat Commun 2019;10:5106. https://doi.org/10.1038/s41467-019-13092-7.

[28] Esswein AJ, Surendranath Y, Reece SY, Nocera DG. Highly active cobalt phosphate and borate based oxygen evolving catalysts operating in neutral and natural waters. Energy Environ Sci 2011;4:499–504. https://doi.org/10.1039/C0EE00518E.

[29] Dresp S, Dionigi F, Loos S, Ferreira de Araujo J, Spöri C, Gliech M, et al. Direct Electrolytic Splitting of Seawater: Activity, Selectivity, Degradation, and Recovery Studied from the Molecular Catalyst Structure to the Electrolyzer Cell Level. Adv Energy Mater 2018;8:1800338. https://doi.org/10.1002/aenm.201800338.

[30] Miles MH. Periodic Variations of Overvoltages for Water Electrolysis in Acid Solutions from Cyclic Voltammetric Studies. J Electrochem Soc 1976;123:1459. https://doi.org/10.1149/1.2132619.

[31] Burke MS, Enman LJ, Batchellor AS, Zou S, Boettcher SW. Oxygen Evolution Reaction Electrocatalysis on Transition Metal Oxides and (Oxy)hydroxides: Activity Trends and Design Principles. Chem Mater 2015;27:7549–58. https://doi.org/10.1021/acs.chemmater.5b03148.

[32] Verbruggen SW. TiO2 photocatalysis for the degradation of pollutants in gas phase:

From morphological design to plasmonic enhancement. J Photochem Photobiol C Photochem Rev 2015;24:64–82. https://doi.org/https://doi.org/10.1016/j.jphotochemrev.2015.07.001.

[33] Liao C-H, Huang CW, C. S. Wu J. Hydrogen Production from Semiconductor-based Photocatalysis via Water Splitting. vol. 2. 2012. https://doi.org/10.3390/catal2040490.

[34] Fujishima A, Honda K. Electrochemical Photolysis of Water at a Semiconductor Electrode. Nature 1972;238:37–8. https://doi.org/10.1038/238037a0.

[35] Van Gerven T, Mul G, Moulijn J, Stankiewicz A. A review of intensification of photocatalytic processes. Chem Eng Process Process Intensif 2007;46:781–9. https://doi.org/https://doi.org/10.1016/j.cep.2007.05.012.

[36] Verbruggen SW, Keulemans M, Filippousi M, Flahaut D, Van Tendeloo G, Lacombe S, et al. Plasmonic gold–silver alloy on TiO2 photocatalysts with tunable visible light activity. Appl Catal B Environ 2014;156–157:116–21. https://doi.org/https://doi.org/10.1016/j.apcatb.2014.03.027.

[37] Acar C, Dincer I, Naterer GF. Review of photocatalytic water-splitting methods for sustainable hydrogen production. Int J Energy Res 2016;40:1449–73. https://doi.org/10.1002/er.3549.

[38] Mohapatra SK, Misra M, Mahajan VK, Raja KS. Design of a Highly Efficient Photoelectrolytic Cell for Hydrogen Generation by Water Splitting: Application of TiO2-xCx Nanotubes as a Photoanode and Pt/TiO2 Nanotubes as a Cathode. J Phys Chem C 2007;111:8677–85. https://doi.org/10.1021/jp071906v.

[39] Luo J, Steier L, Son M-K, Schreier M, Mayer MT, Grätzel M. Cu2O Nanowire Photocathodes for Efficient and Durable Solar Water Splitting. Nano Lett 2016;16:1848–57. https://doi.org/10.1021/acs.nanolett.5b04929.

[40] Chen J, Yang D, Song D, Jiang J, Ma A, Hu MZ, et al. Recent progress in enhancing solar-to-hydrogen efficiency. J Power Sources 2015;280:649–66. https://doi.org/https://doi.org/10.1016/j.jpowsour.2015.01.073.

[41] Li R, Li C. Chapter One - Photocatalytic Water Splitting on Semiconductor-Based Photocatalysts. In: Song C, editor. Adv. Catal., vol. 60, Academic Press; 2017, p. 1–57. https://doi.org/https://doi.org/10.1016/bs.acat.2017.09.001.

[42] International Energy Agency. Technology Roadmap - Hydrogen and Fuel Cells. Paris: 2015.

[43] Pinaud BA, Benck JD, Seitz LC, Forman AJ, Chen Z, Deutsch TG, et al. Technical and economic feasibility of centralized facilities for solar hydrogen production via photocatalysis and photoelectrochemistry. Energy Environ Sci 2013;6:1983–2002. https://doi.org/10.1039/C3EE40831K.

[44] Glenk G, Reichelstein S. Economics of converting renewable power to hydrogen. Nat Energy 2019;4:216–22. https://doi.org/10.1038/s41560-019-0326-1.

[45] Nicodemus JH. Technological learning and the future of solar H2: A component learning comparison of solar thermochemical cycles and electrolysis with solar PV. Energy Policy 2018;120:100–9. https://doi.org/https://doi.org/10.1016/j.enpol.2018.04.072.

[46] Kuang Y, Kenney MJ, Meng Y, Hung W-H, Liu Y, Huang JE, et al. Solar-driven, highly sustained splitting of seawater into hydrogen and oxygen fuels. Proc Natl Acad Sci 2019;116:6624–9. https://doi.org/10.1073/pnas.1900556116.

[47] Dionigi F, Reier T, Pawolek Z, Gliech M, Strasser P. Design Criteria, Operating Conditions, and Nickel–Iron Hydroxide Catalyst Materials for Selective Seawater

Electrolysis. ChemSusChem 2016;9:962–72. https://doi.org/10.1002/cssc.201501581.

[48] Davis JT, Qi J, Fan X, Bui JC, Esposito D V. Floating membraneless PV-electrolyzer based on buoyancy-driven product separation. Int J Hydrogen Energy 2018;43:1224–38. https://doi.org/https://doi.org/10.1016/j.ijhydene.2017.11.086.

[49] Guan X, Chowdhury FA, Pant N, Guo L, Vayssieres L, Mi Z. Efficient Unassisted Overall Photocatalytic Seawater Splitting on GaN-Based Nanowire Arrays. J Phys Chem C 2018;122:13797–802. https://doi.org/10.1021/acs.jpcc.8b00875.

[50] Zhang Y, Li P, Yang X, Fa W, Ge S. High-efficiency and stable alloyed nickel based electrodes for hydrogen evolution by seawater splitting. J Alloys Compd 2018;732:248–56. https://doi.org/https://doi.org/10.1016/j.jallcom.2017.10.194.

[51] Zheng J, Zhao Y, Xi H, Li C. Seawater splitting for hydrogen evolution by robust electrocatalysts from secondary M (M = Cr, Fe, Co, Ni, Mo) incorporated Pt. RSC Adv 2018;8:9423–9. https://doi.org/10.1039/C7RA12112A.

[52] Lu X, Pan J, Lovell E, Tan TH, Ng YH, Amal R. A sea-change: manganese doped nickel/nickel oxide electrocatalysts for hydrogen generation from seawater. Energy Environ Sci 2018;11:1898–910. https://doi.org/10.1039/C8EE00976G.

[53] Miao J, Xiao F-X, Yang H Bin, Khoo SY, Chen J, Fan Z, et al. Hierarchical Ni-Mo-S nanosheets on carbon fiber cloth: A flexible electrode for efficient hydrogen generation in neutral electrolyte. Sci Adv 2015;1:e1500259. https://doi.org/10.1126/sciadv.1500259.

[54] Song LJ, Meng HM. Effect of carbon content on Ni–Fe–C electrodes for hydrogen evolution reaction in seawater. Int J Hydrogen Energy 2010;35:10060–6. https://doi.org/https://doi.org/10.1016/j.ijhydene.2010.08.003.

[55] Zhao Y, Tang Q, He B, Yang P. Carbide decorated carbon nanotube electrocatalyst for high-efficiency hydrogen evolution from seawater. RSC Adv 2016;6:93267–74. https://doi.org/10.1039/C6RA17839A.

[56] Zhao Y, Jin B, Zheng Y, Jin H, Jiao Y, Qiao S-Z. Charge State Manipulation of Cobalt Selenide Catalyst for Overall Seawater Electrolysis. Adv Energy Mater 2018;8:1801926. https://doi.org/10.1002/aenm.201801926.

[57] Ma Y-Y, Wu C-X, Feng X-J, Tan H-Q, Yan L-K, Liu Y, et al. Highly efficient hydrogen evolution from seawater by a low-cost and stable CoMoP@C electrocatalyst superior to Pt/C. Energy Environ Sci 2017;10:788–98. https://doi.org/10.1039/C6EE03768B.

[58] Gao S, Li G-D, Liu Y, Chen H, Feng L-L, Wang Y, et al. Electrocatalytic H2 production from seawater over Co, N-codoped nanocarbons. Nanoscale 2015;7:2306–16. https://doi.org/10.1039/C4NR04924A.

[59] Jin H, Liu X, Vasileff A, Jiao Y, Zhao Y, Zheng Y, et al. Single-Crystal Nitrogen-Rich Two-Dimensional Mo5N6 Nanosheets for Efficient and Stable Seawater Splitting. ACS Nano 2018;12:12761–9. https://doi.org/10.1021/acsnano.8b07841.

[60] Martindale BCM, Reisner E. Bi-Functional Iron-Only Electrodes for Efficient Water Splitting with Enhanced Stability through In Situ Electrochemical Regeneration. Adv Energy Mater 2016;6:1502095. https://doi.org/10.1002/aenm.201502095.

[61] Hsu S-H, Miao J, Zhang L, Gao J, Wang H, Tao H, et al. An Earth-Abundant Catalyst-Based Seawater Photoelectrolysis System with 17.9% Solar-to-Hydrogen Efficiency. Adv Mater 2018;30:1707261. https://doi.org/10.1002/adma.201707261.

[62] Vos JG, Wezendonk TA, Jeremiasse AW, Koper MTM. MnOx/IrOx as Selective Oxygen Evolution Electrocatalyst in Acidic Chloride Solution. J Am Chem Soc 2018;140:10270–81. https://doi.org/10.1021/jacs.8b05382.

[63] Wang Q, Hisatomi T, Jia Q, Tokudome H, Zhong M, Wang C, et al. Scalable water splitting on particulate photocatalyst sheets with a solar-to-hydrogen energy conversion efficiency exceeding 1%. Nat Mater 2016;15:611–5. https://doi.org/10.1038/nmat4589.

[64] Dotan H, Mathews N, Hisatomi T, Grätzel M, Rothschild A. On the Solar to Hydrogen Conversion Efficiency of Photoelectrodes for Water Splitting. J Phys Chem Lett 2014;5:3330–4. https://doi.org/10.1021/jz501716g.

[65] Chen S, Takata T, Domen K. Particulate photocatalysts for overall water splitting. Nat Rev Mater 2017;2:17050. https://doi.org/10.1038/natrevmats.2017.50.

[66] Liu J, Liu Y, Liu N, Han Y, Zhang X, Huang H, et al. Metal-free efficient photocatalyst for stable visible water splitting via a two-electron pathway. Science (80-) 2015;347:970– 4. https://doi.org/10.1126/science.aaa3145.

[67] Liao L, Zhang Q, Su Z, Zhao Z, Wang Y, Li Y, et al. Efficient solar water-splitting using a nanocrystalline CoO photocatalyst. Nat Nanotechnol 2014;9:69–73. https://doi.org/10.1038/nnano.2013.272.

[68] Yang C, Qin J, Rajendran S, Zhang X, Liu R. WS2 and C-TiO2 Nanorods Acting as Effective Charge Separators on g-C3N4 to Boost Visible-Light Activated Hydrogen Production from Seawater. ChemSusChem 2018;11:4077–85. https://doi.org/10.1002/cssc.201801819.

[69] Li F, Dong B, Feng S. Bi shell-BiOI core microspheres modified TiO2 nanotube arrays photoanode: Improved effect of Bi shell on photoelectrochemical hydrogen evolution in seawater. Int J Hydrogen Energy 2019;44:29986–99. https://doi.org/https://doi.org/10.1016/j.ijhydene.2019.09.210.

[70] Nam W, Oh S, Joo H, Yoon J. Preparation of Pt deposited nanotubular TiO2 as cathodes for enhanced photoelectrochemical hydrogen production using seawater electrolytes. J Solid State Chem 2011;184:2920–4. https://doi.org/https://doi.org/10.1016/j.jssc.2011.08.041.

[71] Li Z, Luo W, Zhang M, Feng J, Zou Z. Photoelectrochemical cells for solar hydrogen production: current state of promising photoelectrodes, methods to improve their properties, and outlook. Energy Environ Sci 2013;6:347–70. https://doi.org/10.1039/C2EE22618A.

[72] DOE. FY 2018 Progress Report for the DOE Hydrogen and Fuel Cells Program. 2019.

[73] Guo L, Yang Z, Marcus K, Li Z, Luo B, Zhou L, et al. MoS2/TiO2 heterostructures as nonmetal plasmonic photocatalysts for highly efficient hydrogen evolution. Energy Environ Sci 2018;11:106–14. https://doi.org/10.1039/C7EE02464A.

[74] Simamora A-J, Hsiung T-L, Chang F-C, Yang T-C, Liao C-Y, Wang HP. Photocatalytic splitting of seawater and degradation of methylene blue on CuO/nano TiO2. Int J Hydrogen Energy 2012;37:13855–8. https://doi.org/https://doi.org/10.1016/j.ijhydene.2012.04.091.

[75] Ji SM, Jun H, Jang JS, Son HC, Borse PH, Lee JS. Photocatalytic hydrogen production from natural seawater. J Photochem Photobiol A Chem 2007;189:141–4. https://doi.org/https://doi.org/10.1016/j.jphotochem.2007.01.011.

[76] Sakurai H, Kiuchi M, Jin T. Pt/TiO2 granular photocatalysts for hydrogen production from aqueous glycerol solution: Durability against seawater constituents and dissolved oxygen. Catal Commun 2018;114:124–8. https://doi.org/https://doi.org/10.1016/j.catcom.2018.06.013.

[77] Li Y, He F, Peng S, Gao D, Lu G, Li S. Effects of electrolyte NaCl on photocatalytic

hydrogen evolution in the presence of electron donors over Pt/TiO2. J Mol Catal A Chem 2011;341:71–6. https://doi.org/https://doi.org/10.1016/j.molcata.2011.03.026.

[78] Song T, Zhang P, Wang T, Ali A, Zeng H. Constructing a novel strategy for controllable synthesis of corrosion resistant Ti3+ self-doped titanium–silicon materials with efficient hydrogen evolution activity from simulated seawater. Nanoscale 2018;10:2275–84. https://doi.org/10.1039/C7NR07095K.

[79] Harada H. Isolation of hydrogen from water and/or artificial seawater by sonophotocatalysis using alternating irradiation method. Int J Hydrogen Energy 2001;26:303–7. https://doi.org/https://doi.org/10.1016/S0360-3199(00)00095-1.

[80] Gao M, Connor PKN, Ho GW. Plasmonic photothermic directed broadband sunlight harnessing for seawater catalysis and desalination. Energy Environ Sci 2016;9:3151–60. https://doi.org/10.1039/C6EE00971A.

[81] Husin H, Pontas K, Yunardi, Salamun A, Alam PN, Hasfita F. Photocatalytic hydrogen production over Ni/La-NaTao3 nanoparticles from NaCl-water solution in the presence of glucose as electron donor. ASEAN J Chem Eng 2017;17:27–36. https://doi.org/10.22146/ajche.49553.

[82] Li Y, Lin S, Peng S, Lu G, Li S. Modification of ZnS1−x−0.5yOx(OH)y–ZnO photocatalyst with NiS for enhanced visible-light-driven hydrogen generation from seawater. Int J Hydrogen Energy 2013;38:15976–84. https://doi.org/https://doi.org/10.1016/j.ijhydene.2013.09.149.

[83] Yang T-C, Chang F-C, Wang HP, Wei Y-L, Jou C-J. Photocatalytic splitting of seawater effected by (Ni–ZnO)@C nanoreactors. Mar Pollut Bull 2014;85:696–9. https://doi.org/https://doi.org/10.1016/j.marpolbul.2014.02.011.

[84] Li Y, Gao D, Peng S, Lu G, Li S. Photocatalytic hydrogen evolution over Pt/Cd0.5Zn0.5S from saltwater using glucose as electron donor: An investigation of the influence of electrolyte NaCl. Int J Hydrogen Energy 2011;36:4291–7. https://doi.org/https://doi.org/10.1016/j.ijhydene.2011.01.038.

[85] Ayyub MM, Chhetri M, Gupta U, Roy A, Rao CNR. Photochemical and Photoelectrochemical Hydrogen Generation by Splitting Seawater. Chem – A Eur J 2018;24:18455–62. https://doi.org/10.1002/chem.201804119.

[86] Zhu C, Liu C, Fu Y, Gao J, Huang H, Liu Y, et al. Construction of CDs/CdS photocatalysts for stable and efficient hydrogen production in water and seawater. Appl Catal B Environ 2019;242:178–85. https://doi.org/https://doi.org/10.1016/j.apcatb.2018.09.096.

[87] Qiu B, Zhu Q, Xing M, Zhang J. A robust and efficient catalyst of CdxZn1−xSe motivated by CoP for photocatalytic hydrogen evolution under sunlight irradiation. Chem Commun 2017;53:897–900. https://doi.org/10.1039/C6CC08311K.

[88] Patel M, Park W-H, Ray A, Kim J, Lee J-H. Photoelectrocatalytic sea water splitting using Kirkendall diffusion grown functional Co3O4 film. Sol Energy Mater Sol Cells 2017;171:267–74. https://doi.org/https://doi.org/10.1016/j.solmat.2017.06.058.

[89] Kawde A, Annamalai A, Amidani L, Boniolo M, Kwong WL, Sellstedt A, et al. Photo-electrochemical hydrogen production from neutral phosphate buffer and seawater using micro-structured p-Si photo-electrodes functionalized by solution-based methods. Sustain Energy Fuels 2018;2:2215–23. https://doi.org/10.1039/C8SE00291F.

[90] Ichikawa S. Photoelectrocatalytic production of hydrogen from natural seawater under sunlight. Int J Hydrogen Energy 1997;22:675–8. https://doi.org/https://doi.org/10.1016/S0360-3199(96)00236-4.

[91] Boonserm A, Kruehong C, Seithtanabutara V, Artnaseaw A, Kwakhong P. Photoelectrochemical response and corrosion behavior of CdS/TiO2 nanocomposite films in an aerated 0.5M NaCl solution. Appl Surf Sci 2017;419:933–41. https://doi.org/https://doi.org/10.1016/j.apsusc.2017.05.093.

[92] Yuan X, Xu Y, Meng H, Han Y, Wu J, Xu J, et al. Fabrication of ternary polyaniline-graphene oxide-TiO2 hybrid films with enhanced activity for photoelectrocatalytic hydrogen production. Sep Purif Technol 2018;193:358–67. https://doi.org/https://doi.org/10.1016/j.seppur.2017.10.038.

[93] Li Y, Wang R, Li H, Wei X, Feng J, Liu K, et al. Efficient and Stable Photoelectrochemical Seawater Splitting with TiO2@g-C3N4 Nanorod Arrays Decorated by Co-Pi. J Phys Chem C 2015;119:20283–92. https://doi.org/10.1021/acs.jpcc.5b05427.

[94] Shi Y, Li Y, Wei X, Feng J, Li H, Zhou W. Facile Preparation of Porous WO3 Film for Photoelectrochemical Splitting of Natural Seawater. J Electron Mater 2017;46:6878–83. https://doi.org/10.1007/s11664-017-5730-3.

[95] Jadwiszczak M, Jakubow-Piotrowska K, Kedzierzawski P, Bienkowski K, Augustynski J. Highly Efficient Sunlight-Driven Seawater Splitting in a Photoelectrochemical Cell with Chlorine Evolved at Nanostructured WO3 Photoanode and Hydrogen Stored as Hydride within Metallic Cathode. Adv Energy Mater 2020;10:1903213. https://doi.org/10.1002/aenm.201903213.

[96] Li Y, Feng J, Li H, Wei X, Wang R, Zhou A. Photoelectrochemical splitting of natural seawater with α-Fe2O3/WO3 nanorod arrays. Int J Hydrogen Energy 2016;41:4096–105. https://doi.org/https://doi.org/10.1016/j.ijhydene.2016.01.027.

[97] Liu J, Xu S-M, Li Y, Zhang R, Shao M. Facet engineering of WO3 arrays toward highly efficient and stable photoelectrochemical hydrogen generation from natural seawater. Appl Catal B Environ 2020;264:118540. https://doi.org/https://doi.org/10.1016/j.apcatb.2019.118540.

[98] Li Y, Wei X, Yan X, Cai J, Zhou A, Yang M, et al. Construction of inorganic–organic 2D/2D WO3/g-C3N4 nanosheet arrays toward efficient photoelectrochemical splitting of natural seawater. Phys Chem Chem Phys 2016;18:10255–61. https://doi.org/10.1039/C6CP00353B.

[99] Luo W, Yang Z, Li Z, Zhang J, Liu J, Zhao Z, et al. Solar hydrogen generation from seawater with a modified BiVO4 photoanode. Energy Environ Sci 2011;4:4046–51. https://doi.org/10.1039/C1EE01812D.

[100] Cheng K-W, Tsai W-T, Wu Y-H. Photo-enhanced salt-water splitting using orthorhombic Ag8SnS6 photoelectrodes in photoelectrochemical cells. J Power Sources 2016;317:81–92. https://doi.org/https://doi.org/10.1016/j.jpowsour.2016.03.086.

[101] Zhao X, Zhang G, Zhang Z. TiO2-based catalysts for photocatalytic reduction of aqueous oxyanions: State-of-the-art and future prospects. Environ Int 2020;136:105453. https://doi.org/https://doi.org/10.1016/j.envint.2019.105453.

[102] Ghassemzadeh F, Sherwood J, Geddes MC, Williams WD. The analysis of nitrate in highly saline waters. Int J Salt Lake Res 1997;6:269–78. https://doi.org/10.1007/BF02449929.

[103] Dionex. Determination of Iodide and Iodate in Seawater and Iodized Table Salt by HPLC with UV Detection. 2009.

[104] Zillich JA. Toxicity of Combined Chlorine Residuals to Freshwater Fish. J (Water Pollut Control Fed 1972;44:212–20.

[105] Bennett JE. Electrodes for generation of hydrogen and oxygen from seawater. Int J Hydrogen Energy 1980;5:401–8. https://doi.org/https://doi.org/10.1016/0360-3199(80)90021-X.

[106] Kuhn AT, Chan CY. pH changes at near-electrode surfaces. J Appl Electrochem 1983;13:189–207. https://doi.org/10.1007/BF00612481.

[107] Kato Z, Sato M, Sasaki Y, Izumiya K, Kumagai N, Hashimoto K. Electrochemical characterization of degradation of oxygen evolution anode for seawater electrolysis. Electrochim Acta 2014;116:152–7. https://doi.org/https://doi.org/10.1016/j.electacta.2013.10.014.

[108] Fujimura K, Matsui T, Izumiya K, Kumagai N, Akiyama E, Habazaki H, et al. Oxygen evolution on manganese–molybdenum oxide anodes in seawater electrolysis. Mater Sci Eng A 1999;267:254–9. https://doi.org/https://doi.org/10.1016/S0921-5093(99)00100-8.

[109] Izumiya K, Akiyama E, Habazaki H, Kumagai N, Kawashima A, Hashimoto K. Anodically deposited manganese oxide and manganese–tungsten oxide electrodes for oxygen evolution from seawater. Electrochim Acta 1998;43:3303–12. https://doi.org/https://doi.org/10.1016/S0013-4686(98)00075-9.

[110] Habazaki H, Matsui T, Kawashima A, Asami K, Kumagai N, Hashimoto K. Nanocrystalline manganese-molybdenum-tungsten oxide anodes for oxygen evolution in seawater electrolysis. NANO 2000 Nanostructured Mater Int Conf (5 ; Sendai 2000-08-20) 2001;44:1659–62.

[111] Abdel Ghany NA, Kumagai N, Meguro S, Asami K, Hashimoto K. Oxygen evolution anodes composed of anodically deposited Mn–Mo–Fe oxides for seawater electrolysis. Electrochim Acta 2002;48:21–8. https://doi.org/https://doi.org/10.1016/S0013-4686(02)00539-X.

[112] El-Moneim AA, Kumagai N, Hashimoto K. Mn-Mo-W Oxide Anodes for Oxygen Evolution in Seawater Electrolysis for Hydrogen Production. Mater Trans 2009;50:1969–77. https://doi.org/10.2320/matertrans.M2009107.

[113] Vos JG, Koper MTM. Measurement of competition between oxygen evolution and chlorine evolution using rotating ring-disk electrode voltammetry. J Electroanal Chem 2018;819:260–8. https://doi.org/https://doi.org/10.1016/j.jelechem.2017.10.058.

[114] El-Moneim AA. Mn–Mo–W-oxide anodes for oxygen evolution during seawater electrolysis for hydrogen production: Effect of repeated anodic deposition. Int J Hydrogen Energy 2011;36:13398–406. https://doi.org/https://doi.org/10.1016/j.ijhydene.2011.07.100.

[115] Balaji R, Kannan BS, Lakshmi J, Senthil N, Vasudevan S, Sozhan G, et al. An alternative approach to selective sea water oxidation for hydrogen production. Electrochem Commun 2009;11:1700–2. https://doi.org/10.1016/j.elecom.2009.06.022.

[116] Amikam G, Nativ P, Gendel Y. Chlorine-free alkaline seawater electrolysis for hydrogen production. Int J Hydrogen Energy 2018;43:6504–14. https://doi.org/10.1016/j.ijhydene.2018.02.082.

[117] Kumari S, Turner White R, Kumar B, Spurgeon JM. Solar hydrogen production from seawater vapor electrolysis. Energy Environ Sci 2016;9:1725–33. https://doi.org/10.1039/C5EE03568F.

[118] Lair A, Ferronato C, Chovelon J-M, Herrmann J-M. Naphthalene degradation in water by heterogeneous photocatalysis: An investigation of the influence of inorganic anions. J Photochem Photobiol A Chem 2008;193:193–203.

https://doi.org/https://doi.org/10.1016/j.jphotochem.2007.06.025.

[119] Cooper WJ, Jones AC, Whitehead RF, Zika RG. Sunlight-Induced Photochemical Decay of Oxidants in Natural Waters: Implications in Ballast Water Treatment. Environ Sci Technol 2007;41:3728–33. https://doi.org/10.1021/es062975a.

[120] Song T-T, Su T-M. Recombination Reactions of Atomic Chlorine in Compressed Gases. 2. Geminate and Nongeminate Recombinations and Photolysis Quantum Yields with Argon Pressure Up to 180 bar. J Phys Chem 1996;100:13554–60. https://doi.org/10.1021/jp9605008.

[121] Bertus LM, Carcel RA. Prediction of TiO2 and WO3 nanopowders surface charge by the evaluation of point of zero charge (PZC). Environ Eng Manag J 2011;10:1021–6. https://doi.org/10.30638/eemj.2011.148.

[122] Maeda K, Masuda H, Domen K. Effect of electrolyte addition on activity of (Ga1−xZnx)(N1−xOx) photocatalyst for overall water splitting under visible light. Catal Today 2009;147:173–8. https://doi.org/https://doi.org/10.1016/j.cattod.2008.09.002.

[123] Solarska R, Alexander BD, Braun A, Jurczakowski R, Fortunato G, Stiefel M, et al. Tailoring the morphology of WO3 films with substitutional cation doping: Effect on the photoelectrochemical properties. Electrochim Acta 2010;55:7780–7. https://doi.org/https://doi.org/10.1016/j.electacta.2009.12.016.

[124] Zhang LA. Removal of Chlorine Residual in Tap Water by Boiling or Adding Ascorbic Acid. Int J Eng Res Appl 2013;3:1647–51.

[125] Seger B, Kamat P V. Fuel Cell Geared in Reverse: Photocatalytic Hydrogen Production Using a TiO2/Nafion/Pt Membrane Assembly with No Applied Bias. J Phys Chem C 2009;113:18946–52. https://doi.org/10.1021/jp907367k.

[126] Verbruggen SW, Van Hal M, Bosserez T, Rongé J, Hauchecorne B, Martens JA, et al. Harvesting Hydrogen Gas from Air Pollutants with an Unbiased Gas Phase Photoelectrochemical Cell. ChemSusChem 2017;10:1413–8. https://doi.org/10.1002/cssc.201601806.

[127] Surendranath Y, Dincă M, Nocera DG. Electrolyte-Dependent Electrosynthesis and Activity of Cobalt-Based Water Oxidation Catalysts. J Am Chem Soc 2009;131:2615–20. https://doi.org/10.1021/ja807769r.

[128] Rashid MM, Mesfer MK Al, Naseem H, Danish M. Hydrogen Production by Water Electrolysis: A Review of Alkaline Water Electrolysis, PEM Water Electrolysis and High Temperature Water Electrolysis. Int J Eng Adv Technol 2015;4:2249–8958.

[129] Schalenbach M, Hoefner T, Paciok P, Carmo M, Lueke W, Stolten D. Gas Permeation through Nafion. Part 1: Measurements. J Phys Chem C 2015;119:25145–55. https://doi.org/10.1021/acs.jpcc.5b04155.

[130] Li H, Tang Q, He B, Yang P. Robust electrocatalysts from an alloyed Pt–Ru–M (M = Cr, Fe, Co, Ni, Mo)-decorated Ti mesh for hydrogen evolution by seawater splitting. J Mater Chem A 2016;4:6513–20. https://doi.org/10.1039/C6TA00785F.

[131] Kirk DW, Ledas AE. Precipitate formation during sea water electrolysis. Int J Hydrogen Energy 1982;7:925–32. https://doi.org/https://doi.org/10.1016/0360-3199(82)90160-4.

[132] Kapp EMK. The precipitation of calcium and magnesium from sea water by sodium hydroxide. Biol Bull 1928;55:453–8.

[133] Esposito D V. Membrane-Coated Electrocatalysts—An Alternative Approach To Achieving Stable and Tunable Electrocatalysis. ACS Catal 2018;8:457–65. https://doi.org/10.1021/acscatal.7b03374.

[134] Oh BS, Oh SG, Hwang YY, Yu H-W, Kang J-W, Kim IS. Formation of hazardous inorganic by-products during electrolysis of seawater as a disinfection process for desalination. Sci Total Environ 2010;408:5958–65. https://doi.org/https://doi.org/10.1016/j.scitotenv.2010.08.057.

[135] Makhlouf ASH, Botello MA. Chapter 1 - Failure of the metallic structures due to microbiologically induced corrosion and the techniques for protection. In: Makhlouf ASH, Aliofkhazraei M, editors., Butterworth-Heinemann; 2018, p. 1–18. https://doi.org/https://doi.org/10.1016/B978-0-08-101928-3.00001-X.

[136] Ito H, Maeda T, Nakano A, Takenaka H. Properties of Nafion membranes under PEM water electrolysis conditions. Int J Hydrogen Energy 2011;36:10527–40. https://doi.org/https://doi.org/10.1016/j.ijhydene.2011.05.127.

[137] Labrador NY, Songcuan EL, De Silva C, Chen H, Kurdziel SJ, Ramachandran RK, et al. Hydrogen Evolution at the Buried Interface between Pt Thin Films and Silicon Oxide Nanomembranes. ACS Catal 2018;8:1767–78. https://doi.org/10.1021/acscatal.7b02668.

[138] Siwińska-Stefańska K, Kubiaka A, Piasecki A, Goscianska J, Nowaczyk G, Jurga S, et al. TiO_2-ZnO Binary Oxide Systems: Comprehensive Characterization and Tests of Photocatalytic Activity. Mater (Basel, Switzerland) 2018;11:841. https://doi.org/10.3390/ma11050841.

[139] Takata T, Pan C, Domen K. Recent progress in oxynitride photocatalysts for visible-light-driven water splitting. Sci Technol Adv Mater 2015;16:33506. https://doi.org/10.1088/1468-6996/16/3/033506.

[140] Takata T, Pan C, Domen K. Design and Development of Oxynitride Photocatalysts for Overall Water Splitting under Visible Light Irradiation. ChemElectroChem 2016;3:31–7. https://doi.org/10.1002/celc.201500324.

[141] Ishikawa A, Takata T, Kondo JN, Hara M, Kobayashi H, Domen K. Oxysulfide Sm2Ti2S2O5 as a Stable Photocatalyst for Water Oxidation and Reduction under Visible Light Irradiation ($\lambda \leq 650$ nm). J Am Chem Soc 2002;124:13547–53. https://doi.org/10.1021/ja0269643.

[142] Liu Y, Yu Y-X, Zhang W-D. MoS2/CdS Heterojunction with High Photoelectrochemical Activity for H2 Evolution under Visible Light: The Role of MoS2. J Phys Chem C 2013;117:12949–57. https://doi.org/10.1021/jp4009652.

[143] Meng X, Zhang Z. Pd-doped Bi2MoO6 plasmonic photocatalysts with enhanced visible light photocatalytic performance. Appl Surf Sci 2017;392:169–80. https://doi.org/https://doi.org/10.1016/j.apsusc.2016.08.113.

[144] Blommaerts N, Asapu R, Claes N, Bals S, Lenaerts S, Verbruggen SW. Gas phase photocatalytic spiral reactor for fast and efficient pollutant degradation. Chem Eng J 2017;316:850–6. https://doi.org/https://doi.org/10.1016/j.cej.2017.02.038.

[145] Asapu R, Claes N, Bals S, Denys S, Detavernier C, Lenaerts S, et al. Silver-polymer core-shell nanoparticles for ultrastable plasmon-enhanced photocatalysis. Appl Catal B Environ 2017;200:31–8. https://doi.org/https://doi.org/10.1016/j.apcatb.2016.06.062.

[146] Peeters H, Keulemans M, Nuyts G, Vanmeert F, Li C, Minjauw M, et al. Plasmonic gold-embedded TiO2 thin films as photocatalytic self-cleaning coatings. Appl Catal B Environ 2020;267:118654. https://doi.org/https://doi.org/10.1016/j.apcatb.2020.118654.

[147] Caretti I, Keulemans M, Verbruggen SW, Lenaerts S, Van Doorslaer S. Light-Induced

Processes in Plasmonic Gold/TiO2 Photocatalysts Studied by Electron Paramagnetic Resonance. Top Catal 2015;58:776–82. https://doi.org/10.1007/s11244-015-0419-4.

[148] Asapu R, Claes N, Ciocarlan R-G, Minjauw M, Detavernier C, Cool P, et al. Electron Transfer and Near-Field Mechanisms in Plasmonic Gold-Nanoparticle-Modified TiO2 Photocatalytic Systems. ACS Appl Nano Mater 2019;2:4067–74. https://doi.org/10.1021/acsanm.9b00485.

[149] Liao TW, Verbruggen SW, Claes N, Yadav A, Grandjean D, Bals S, et al. TiO2 films modified with au nanoclusters as self-cleaning surfaces under visible light. Nanomaterials 2018;8:1–9. https://doi.org/10.3390/nano8010030.

[150] Verbruggen SW, Keulemans M, Goris B, Blommaerts N, Bals S, Martens JA, et al. Plasmonic 'rainbow' photocatalyst with broadband solar light response for environmental applications. Appl Catal B Environ 2016;188:147–53. https://doi.org/https://doi.org/10.1016/j.apcatb.2016.02.002.

[151] Ni M, Leung MKH, Leung D, Sumathy K. A Review and Recent Developments in Photocatalytic Water-Splitting Using TiO2 for Hydrogen Production. Renew Sustain Energy Rev 2007;11:401–25. https://doi.org/10.1016/j.rser.2005.01.009.

[152] Toutianoush A, Jin W, Deligöz H, Tieke B. Polyelectrolyte multilayer membranes for desalination of aqueous salt solutions and seawater under reverse osmosis conditions. Appl Surf Sci 2005;246:437–43. https://doi.org/https://doi.org/10.1016/j.apsusc.2004.11.068.

[153] Krivec M, Dillert R, Bahnemann DW, Mehle A, Štrancar J, Dražić G. The nature of chlorine-inhibition of photocatalytic degradation of dichloroacetic acid in a TiO2-based microreactor. Phys Chem Chem Phys 2014;16:14867–73. https://doi.org/10.1039/C4CP01043D.

[154] Sayama K, Arakawa H. Effect of carbonate addition on the photocatalytic decomposition of liquid water over a ZrO2 catalyst. J Photochem Photobiol A Chem 1996;94:67–76. https://doi.org/https://doi.org/10.1016/1010-6030(95)04204-0.

[155] Augustynski J, Solarska R, Hagemann H, Santato C. Nanostructured thin-film tungsten trioxide photoanodes for solar water and sea-water splitting. Proc. SPIE - Int. Soc. Opt. Eng., vol. 6340, 2006.

[156] Seabold JA, Choi K-S. Effect of a Cobalt-Based Oxygen Evolution Catalyst on the Stability and the Selectivity of Photo-Oxidation Reactions of a WO3 Photoanode. Chem Mater 2011;23:1105–12. https://doi.org/10.1021/cm1019469.

[157] Li X, Fang X, Pang R, Li J, Sun X, Shen J, et al. Self-assembly of TiO2 nanoparticles around the pores of PES ultrafiltration membrane for mitigating organic fouling. J Memb Sci 2014;467:226–35. https://doi.org/https://doi.org/10.1016/j.memsci.2014.05.036.

[158] Bae T-H, Kim I-C, Tak T-M. Preparation and characterization of fouling-resistant TiO2 self-assembled nanocomposite membranes. J Memb Sci 2006;275:1–5. https://doi.org/https://doi.org/10.1016/j.memsci.2006.01.023.

[159] Kumar M, Gholamvand Z, Morrissey A, Nolan K, Ulbricht M, Lawler J. Preparation and characterization of low fouling novel hybrid ultrafiltration membranes based on the blends of GO–TiO2 nanocomposite and polysulfone for humic acid removal. J Memb Sci 2016;506:38–49. https://doi.org/https://doi.org/10.1016/j.memsci.2016.02.005.

[160] Oh S, Nam W, Joo H, Sarp S, Cho J, Lee C-H, et al. Photoelectrochemical hydrogen production with concentrated natural seawater produced by membrane process. Sol Energy 2011;85:2256–63.

https://doi.org/https://doi.org/10.1016/j.solener.2011.06.013.

[161] Trasatti S. Work function, electronegativity, and electrochemical behaviour of metals: III. Electrolytic hydrogen evolution in acid solutions. J Electroanal Chem Interfacial Electrochem 1972;39:163–84. https://doi.org/https://doi.org/10.1016/S0022-0728(72)80485-6.

[162] Lu Q, Hutchings GS, Yu W, Zhou Y, Forest R V, Tao R, et al. Highly porous non-precious bimetallic electrocatalysts for efficient hydrogen evolution. Nat Commun 2015;6:6567. https://doi.org/10.1038/ncomms7567.

[163] Du X, Yang Q, Chen Y, Yang Y, Zhang Z. Galvanic corrosion behavior of copper/titanium galvanic couple in artificial seawater. Trans Nonferrous Met Soc China 2014;24:570–81. https://doi.org/https://doi.org/10.1016/S1003-6326(14)63097-1.

[164] Patel PP, Hanumantha PJ, Datta MK, Velikokhatnyi OI, Hong D, Poston JA, et al. Cobalt based nanostructured alloys: Versatile high performance robust hydrogen evolution reaction electro-catalysts for electrolytic and photo-electrochemical water splitting. Int J Hydrogen Energy 2017;42:17049–62. https://doi.org/https://doi.org/10.1016/j.ijhydene.2017.05.175.

[165] Patel PP, Velikokhatnyi OI, Ghadge SD, Hanumantha PJ, Datta MK, Kuruba R, et al. Electrochemically active and robust cobalt doped copper phosphosulfide electro-catalysts for hydrogen evolution reaction in electrolytic and photoelectrochemical water splitting. Int J Hydrogen Energy 2018;43:7855–71. https://doi.org/https://doi.org/10.1016/j.ijhydene.2018.02.147.

[166] Simamora AJ, Chang FC, Wang HP, Yang TC, Wei YL, Lin WK. H2 fuels from photocatalytic splitting of seawater affected by nano-TiO2 promoted with CuO and NiO. Int J Photoenergy 2013;2013:1–6. https://doi.org/10.1155/2013/419182.

[167] Speltini A, Scalabrini A, Maraschi F, Sturini M, Pisanu A, Malavasi L, et al. Improved photocatalytic H2 production assisted by aqueous glucose biomass by oxidized g-C3N4. Int J Hydrogen Energy 2018;43:14925–33. https://doi.org/https://doi.org/10.1016/j.ijhydene.2018.06.103.

[168] Mishra B, Mishra S, Satpati B, Chaudhary YS. Engineering the Surface of a Polymeric Photocatalyst for Stable Solar-to-Chemical Fuel Conversion from Seawater. ChemSusChem 2019;12:3383–9. https://doi.org/https://doi.org/10.1002/cssc.201900388.

[169] Liu Y, Liao Z, Ma X, Xiang Z. Ultrastable and Efficient Visible-Light-Driven Hydrogen Production Based on Donor–Acceptor Copolymerized Covalent Organic Polymer. ACS Appl Mater Interfaces 2018;10:30698–705. https://doi.org/10.1021/acsami.8b10022.

[170] Liu Y, Xiang Z. Fully Conjugated Covalent Organic Polymer with Carbon-Encapsulated Ni2P for Highly Sustained Photocatalytic H2 Production from Seawater. ACS Appl Mater Interfaces 2019;11:41313–20. https://doi.org/10.1021/acsami.9b13540.

[171] Li L, Zhou Z, Li L, Zhuang Z, Bi J, Chen J, et al. Thioether-Functionalized 2D Covalent Organic Framework Featuring Specific Affinity to Au for Photocatalytic Hydrogen Production from Seawater. ACS Sustain Chem Eng 2019;7:18574–81. https://doi.org/10.1021/acssuschemeng.9b04749.

[172] Nam W, Oh S, Joo H, Sarp S, Cho J, Nam B-W, et al. Preparation of anodized TiO2 photoanode for photoelectrochemical hydrogen production using natural seawater. Sol Energy Mater Sol Cells 2010;94:1809–15. https://doi.org/https://doi.org/10.1016/j.solmat.2010.05.051.

[173] Dominey RN, Lewis NS, Bruce JA, Bookbinder DC, Wrighton MS. Improvement of

photoelectrochemical hydrogen generation by surface modification of p-type silicon semiconductor photocathodes. J Am Chem Soc 1982;104:467–82. https://doi.org/10.1021/ja00366a016.

[174] Hou Y, Abrams BL, Vesborg PCK, Björketun ME, Herbst K, Bech L, et al. Bioinspired molecular co-catalysts bonded to a silicon photocathode for solar hydrogen evolution. Nat Mater 2011;10:434–8. https://doi.org/10.1038/nmat3008.

[175] Dubale AA, Pan C-J, Tamirat AG, Chen H-M, Su W-N, Chen C-H, et al. Heterostructured Cu2O/CuO decorated with nickel as a highly efficient photocathode for photoelectrochemical water reduction. J Mater Chem A 2015;3:12482–99. https://doi.org/10.1039/C5TA01961C.

[176] Morales-Guio CG, Tilley SD, Vrubel H, Grätzel M, Hu X. Hydrogen evolution from a copper(I) oxide photocathode coated with an amorphous molybdenum sulphide catalyst. Nat Commun 2014;5:3059. https://doi.org/10.1038/ncomms4059.

[177] Sun Y, Liu C, Grauer DC, Yano J, Long JR, Yang P, et al. Electrodeposited Cobalt-Sulfide Catalyst for Electrochemical and Photoelectrochemical Hydrogen Generation from Water. J Am Chem Soc 2013;135:17699–702. https://doi.org/10.1021/ja4094764.

[178] Herzberg M, Elimelech M. Biofouling of reverse osmosis membranes: Role of biofilm-enhanced osmotic pressure. J Memb Sci 2007;295:11–20. https://doi.org/https://doi.org/10.1016/j.memsci.2007.02.024.

[179] Paidar M, Fateev V, Bouzek K. Membrane electrolysis—History, current status and perspective. Electrochim Acta 2016;209:737–56. https://doi.org/https://doi.org/10.1016/j.electacta.2016.05.209.

[180] Parnian MJ, Rowshanzamir S, Alipour Moghaddam J. Investigation of physicochemical and electrochemical properties of recast Nafion nanocomposite membranes using different loading of zirconia nanoparticles for proton exchange membrane fuel cell applications. Mater Sci Energy Technol 2018;1:146–54. https://doi.org/https://doi.org/10.1016/j.mset.2018.06.008.

[181] Kienitz BL, Baskaran H, Zawodzinski TA. Modeling the steady-state effects of cationic contamination on polymer electrolyte membranes. Electrochim Acta 2009;54:1671–9. https://doi.org/https://doi.org/10.1016/j.electacta.2008.09.058.

[182] Oener SZ, Ardo S, Boettcher SW. Ionic Processes in Water Electrolysis: The Role of Ion-Selective Membranes. ACS Energy Lett 2017;2:2625–34. https://doi.org/10.1021/acsenergylett.7b00764.

[183] Lavorante MJ, Reynoso CY, Franco JI. Water electrolysis with Zirfon® as separator and NaOH as electrolyte. Desalin Water Treat 2015;56:3647–53. https://doi.org/10.1080/19443994.2014.974214.

[184] Hisatomi T, Domen K. Introductory lecture: sunlight-driven water splitting and carbon dioxide reduction by heterogeneous semiconductor systems as key processes in artificial photosynthesis. Faraday Discuss 2017;198:11–35. https://doi.org/10.1039/C6FD00221H.

[185] Selli E, Chiarello GL, Quartarone E, Rossetti I, Forni L. A photocatalytic water splitting device for separate hydrogen and oxygen evolution. Chem Commun (Camb) 2008;1:5022–4. https://doi.org/10.1039/b711747g.

[186] Pan C, Takata T, Nakabayashi M, Matsumoto T, Shibata N, Ikuhara Y, et al. A complex perovskite-type oxynitride: the first photocatalyst for water splitting operable at up to 600 nm. Angew Chem Int Ed Engl 2015;54:2955–9. https://doi.org/10.1002/anie.201410961.

[187] DeepanPrakash D, Premnath V, Raghu C, Vishnukumar S, Jayanthi SS, Easwaramoorthy D. Harnessing power from sea water using nano material as photocatalyst and solar energy as light source: the role of hydrocarbon as dual agent. Int J Energy Res 2014;38:249–53. https://doi.org/10.1002/er.3017.

[188] d'Amore-Domenech R, Leo TJ. Sustainable Hydrogen Production from Offshore Marine Renewable Farms: Techno-Energetic Insight on Seawater Electrolysis Technologies. ACS Sustain Chem Eng 2019;7:8006–22. https://doi.org/10.1021/acssuschemeng.8b06779.

[189] Faber C, Allahverdiyeva-Rinne Yagut, Artero V, Baraton Laurent, Barbieri A, Bercegol H, et al. Technological Roadmap Technical Appendix Part 1 - Sustainable Hydrogen Production. 2020. https://doi.org/10.2307/j.ctvc772xh.18.

[190] Styring S. Artificial photosynthesis for solar fuels. Faraday Discuss 2012;155:357–76. https://doi.org/10.1039/C1FD00113B.

[191] Raja KS, Mahajan VK, Misra M. Determination of photo conversion efficiency of nanotubular titanium oxide photo-electrochemical cell for solar hydrogen generation. J Power Sources 2006;159:1258–65. https://doi.org/https://doi.org/10.1016/j.jpowsour.2005.12.036.

[192] Tunesi S, Anderson MA. Photocatalysis of 3,4-DCB in TiO2 aqueous suspensions; effects of temperature and light intensity; CIR-FTIR interfacial analysis. Chemosphere 1987;16:1447–56. https://doi.org/https://doi.org/10.1016/0045-6535(87)90084-1.

1 **TOC Entry**
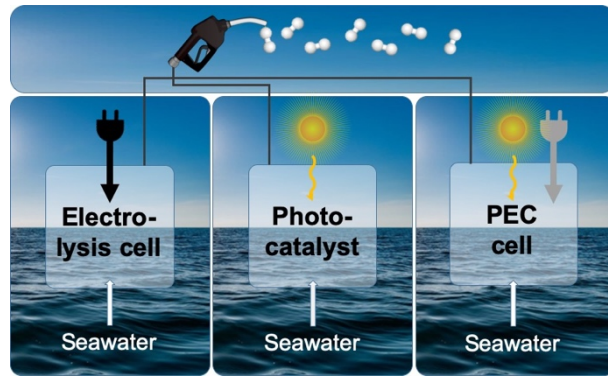
2

3 The pros and cons of electrolytic, photocatalytic and photoelectrochemical seawater splitting are

4 compared, highlighting technological advances and sustainability aspects.